

The brown adipocyte protein CIDEA promotes lipid droplet fusion via a phosphatidic acid-binding amphipathic helix

David Barneda¹, Joan Planas-Iglesias², Maria L. Gaspar³, Dariush Mohammadyani⁴, Sunil Prasannan⁸, Dirk Dormann⁵, Gil-Soo Han⁵, Stephen A. Jesch³, George M. Carman⁶, Valerian Kagan⁴, Malcolm G. Parker¹, Nicholas T. Ktistakis⁷, Judith Klein-Seetharaman^{2,4}, Ann M. Dixon⁸, Susan A. Henry³, Mark Christian^{1,2*}.

¹ Institute of Reproductive and Developmental Biology, Imperial College London, London W12 0NN, UK

² Warwick Medical School, University of Warwick, Coventry, CV4 7AL, UK.

³ Department of Molecular Biology and Genetics, Cornell University, Ithaca, New York 14853, USA.

⁴ Department of Bioengineering, University of Pittsburgh, Pittsburgh, Pennsylvania 15219, USA.

⁵ Microscopy Facility, MRC Clinical Sciences Centre, Imperial College London, London W12 0NN, UK

⁶ Department of Food Science, Rutgers Center for Lipid Research, Rutgers University, New Brunswick, New Jersey 08901, USA.

⁷ Signalling Programme, Babraham Institute, Cambridge CB22 3AT, UK.

⁸ Department of Chemistry, University of Warwick, Coventry, CV4 7AL, UK.

*Corresponding author.

E-mail: m.christian@warwick.ac.uk

Phone number: 44 2476 96 8585

21

22 **Summary**

23 Maintenance of energy homeostasis depends on the highly regulated storage and
24 release of triacylglycerol primarily in adipose tissue and excessive storage is a feature of
25 common metabolic disorders. CIDEA is a lipid droplet (LD)-protein enriched in brown
26 adipocytes promoting the enlargement of LDs which are dynamic, ubiquitous organelles
27 specialized for storing neutral lipids. We demonstrate an essential role in this process for
28 an amphipathic helix in CIDEA, which facilitates embedding in the LD phospholipid
29 monolayer and binds phosphatidic acid (PA). LD pairs are docked by CIDEA trans-
30 complexes through contributions of the N-terminal domain and a C-terminal dimerization
31 region. These complexes, enriched at the LD-LD contact site, interact with the cone-
32 shaped phospholipid PA and likely increase phospholipid barrier permeability, promoting
33 LD fusion by transference of lipids. This physiological process is essential in adipocyte
34 differentiation as well as serving to facilitate the tight coupling of lipolysis and
35 lipogenesis in activated brown fat.

36

37 **Introduction**

38 Evolutionary pressures for survival in fluctuating environments that expose
39 organisms to times of both feast and famine have selected for the ability to efficiently
40 store and release energy in the form of triacylglycerol (TAG). However, excessive or
41 defective lipid storage is a key feature of common diseases such as diabetes,
42 atherosclerosis and the metabolic syndrome (1). The organelles that are essential for
43 storing and mobilizing intracellular fat are lipid droplets (LDs) (2). They constitute a
44 unique cellular structure where a core of neutral lipids is stabilized in the hydrophilic
45 cytosol by a phospholipid monolayer embedding LD-proteins. While most mammalian
46 cells present small LDs ($<1\ \mu\text{m}$) (3), white (unilocular) adipocytes contain a single giant
47 LD occupying most of their cell volume. In contrast, brown (multilocular) adipocytes
48 hold multiple LDs of lesser size, increasing the LD surface/volume ratio which facilitates
49 the rapid consumption of lipids for adaptive thermogenesis (4).

50 The exploration of new approaches for the treatment of metabolic disorders has
51 been stimulated by the rediscovery of active brown adipose tissue (BAT) in adult humans
52 (5, 6) and by the induction of multilocular brown-like cells in white adipose tissue (WAT)
53 (7). The multilocular morphology of brown adipocytes is a defining characteristic of these
54 cells along with expression of genes such as Ucp1. The acquisition of a unilocular or
55 multilocular phenotype is likely to be controlled by the regulation of LD growth. Two
56 related proteins, CIDEA and CIDEC promote LD enlargement in adipocytes (8-10), with
57 CIDEA being specifically found in BAT. Together with CIDEB, they form the CIDE (cell
58 death-inducing DFF45-like effector) family of LD-proteins, which have emerged as
59 important metabolic regulators (11).

60 Different mechanisms have been proposed for LD enlargement, including *in situ*
61 neutral lipid synthesis, lipid uptake and LD-LD coalescence (12-14). The study of CIDE
62 proteins has revealed a critical role in the LD fusion process in which a donor LD
63 progressively transfers its content to an acceptor LD until it is completely absorbed (15).
64 However, the underlying mechanism by which CIDEC and CIDEA facilitate the
65 interchange of triacylglycerol (TAG) molecules between LDs is not understood. In the
66 present study, we have obtained a detailed picture of the different steps driving this LD
67 enlargement process, which involves the stabilization of LD pairs, phospholipid binding,
68 and the permeabilization of the LD monolayer to allow the transference of lipids.

69 **Results**

70 **CIDEA expression mimics the LD dynamics observed during the differentiation of**
71 **brown adipocytes.** To examine the processes controlling LD enlargement in brown
72 adipocytes we followed LD dynamics by time-lapse microscopy. During differentiation
73 of immortalized brown preadipocytes large LDs were formed by the fusion of pre-existing
74 LDs (Video 1). This fusion process was characterized by a slow and progressive reduction
75 in the volume of a donor LD until completely absorbed by an acceptor LD (Fig. 1A),
76 which is characteristic of CIDE activity. As CIDEA is selectively expressed in brown
77 adipocytes and could have a prominent role in the acquisition of their multilocular
78 morphology, we explored the effects of its expression in undifferentiated pre-adipocytes.
79 After inducing CIDEA, LDs in pre-adipocytes showed an equivalent dynamic pattern to
80 that observed in differentiating brown cells, with the progressive fusion of the initial LDs
81 until a few large LDs remained in the cell (Video 2). LD fusion was achieved by the slow
82 transference of lipids between LDs, and was preceded by the formation of small clusters
83 of interacting LDs (Fig. 1B). Given the importance of this process in adipocyte dynamics,
84 we decided to undertake a comprehensive molecular analysis.

Phases of CIDEA activity: LD targeting, LD-LD docking and LD growth. The ectopic expression of full length CIDEA induced the formation of large LDs through LD fusion by lipid transfer (Fig. 1C-D). Control cells lacking expression of CIDEA did not show LD enlargement (Fig 1C). As many proteins are constructed of domains, that are conserved across families and serve as their main structural and functional units, we assessed the conserved regions within the CIDE proteins. By comparing the 217 amino acid (aa) sequence of CIDEA with that of CIDEB and CIDEA, 4 highly conserved regions can be identified (Fig. 2A and Fig. 2-Figure Supplement 1). The N-terminal (N-term) domain of CIDEA is composed of a basic region (2-72 aa) followed by an acidic sequence (73-110 aa). These distinctly differently charged regions are indicated by protein crystallography studies to be important for the dimerization of CIDE domain proteins (16-19). The CIDEA C-terminal (C-term) is rich in basic aas and contains a highly conserved region (126-155 aa), and a basic and hydrophobic sequence (162-197 aa). Based on this sequence analysis, we created an extensive collection of v5-tagged CIDE point and deletion mutants to test their effects on LDs (Fig. 2). Interestingly, certain mutations such as R171E/R175E promoted the aggregation of the cellular LDs in a few “bunch of grapes”-like LD clusters, but were unable to induce the transference of lipids between them (Fig. 2B). In other cases, as with the expression of CIDEA-(116-217)-v5, the LDs remained small and dispersed throughout the cytoplasm despite the protein being normally localized at their surface. Finally, some versions of CIDEA such as CIDEA-(1-118)-v5 showed no LD localization and did not affect their size, number or distribution. Together with the time-lapse results, this indicates that the molecular mechanism of CIDEA is composed by three discrete phases: LD targeting, LD-LD docking, and LD growth.

109 **A cationic amphipathic helix in C-term drives LD targeting.** All the CIDEA
110 constructs that showed impaired LD localization contained deletions or mutations in the
111 C-term hydrophobic and basic region (162-197 aa) (Fig. 2C). In fact, the last 66 aas of
112 CIDEA were sufficient for LD localization, as shown with the expression of CIDEA-
113 (152-217)-v5, whereas it lacked the ability to facilitate the docking of LDs (Fig. 2C and
114 4A). Although it is known that the C-term domain of CIDE proteins is essential for LD
115 localization and enlargement (20, 21), only the structure of the N-term domain has been
116 solved (16-19). The CIDE-N domain (Pfam reference PF02017) has been determined in
117 members of the CIDE family (PBD Codes: 2eel (hCIDEA), 1D4B (hCIDEB), 4MAC
118 (mCIDEA), 4ikg (mCIDEA)), to aas 40-117, 34-100, and 41-118 in hCIDEA, hCIDEB
119 and mCIDEA, respectively. Thus, the sequence 163-180, which we found essential for
120 LD-targeting (Fig. 2C), lacks direct structural information to date. We therefore predicted
121 its structure using *in silico* approaches. The region displayed high probability of a helical
122 conformation, with strongly amphipathic character (Fig. 3A, 3B and Fig. 3-Figure
123 Supplement 1). To experimentally confirm the presence of an amphipathic helix in the LD-
124 targeting domain of CIDEA, Circular Dichroism (CD) spectroscopy was used to estimate
125 the secondary structure of a synthetic peptide corresponding to residues 158-185 in
126 CIDEA. The CD spectra in the presence of 0.1% n-dodecyl- β -D-maltopyranoside
127 confirmed the presence of α -helical structure (Fig. 3C).

128 As some LD proteins are known to be bound to the LD membrane through
129 amphipathic helices (22, 23), we tested if this short sequence was sufficient for LD
130 targeting. While HA-(1-120)-CIDEA showed no LD localization and had no effect on LD
131 distribution or size, HA-CIDEA-(1-117)-(163-180) was partially localized on the LD
132 surface and promoted LD clustering (Fig. 3D). Furthermore, the deletion of this C-term
133 sequence in CIDEA- Δ (163-179)-v5 completely eliminated LD localization in most of the

134 cells (Fig. 2B and Fig. 2C), confirming its role in LD targeting. However, partial LD
135 localization could be observed in a small percentage of cells, together with the presence
136 of LD clusters. This was also observed in CIDEA- Δ (162-197)-v5 and was particularly
137 frequent in CIDEA-(N172X)-v5, which contains a deletion in the middle of the helix. In
138 contrast, no LD-targeting could be observed for the N-term fragment alone (1-118aa) (Fig
139 2C). This may indicate that other regions in C-term may contribute to LD localization,
140 either by directly binding the LD membrane or by interacting with other LD proteins.
141 Similarly, LD targeting was compromised when the amphipathic character of the helix was
142 disrupted in CIDEA-(F166R/V169R/L170R)-v5 by introducing cationic aas in its
143 hydrophobic face. Although LD localization was only lost in a small percentage of cells,
144 in the remaining cells the LD staining was accompanied by a predominantly cytosolic
145 localisation (Fig. 3E and Fig. 2C). In contrast, the predominant LD localization of wild
146 type (wt) CIDEA was maintained in CIDEA-(K167E/R171E/R175E)-v5, which presents
147 a charge inversion of the helix but maintains its amphipathic properties (Fig. 3E and Fig.
148 2C).

149 **The amphipathic helix is essential for LD enlargement.** In addition to its role in LD
150 targeting, our data indicates that the cationic amphipathic helix in the C-term participates
151 in the TAG transference step of CIDEA activity, as the charge inversion
152 (K167E/R171E/R175E) did not affect LD targeting but completely blocked LD
153 enlargement (Fig. 2C). Despite not being essential for LD targeting, the cationic amino
154 acids in the helix are highly conserved in vertebrates (Fig. 3-Figure Supplement 3A).
155 K167 is 100% conserved across all vertebrate species examined. R171 was conserved
156 across vertebrates including birds, snakes, lizards, crocodiles, turtles, marsupials,
157 placental mammals, monotremes, although not in fish. R175 is also highly conserved with
158 only birds, dolphin and Nile Tilapia (a fish) lacking this residue. Remarkably, an

159 amphipathic helix is predicted in CIDEA of all the vertebrate species examined (Fig. 3-
160 Figure Supplement 3B).

161 The absence of negative charges in the helix appeared as essential condition to
162 permit TAG transference, as a single inverted charge mutation such as R171E or R175E
163 was sufficient to block LD enlargement (Fig. 2C). In contrast conservative substitutions
164 such as R171K or K167R did not affect CIDEA activity, and even the substitution of the
165 3 basic aa to histidine in (K167H/R171H/R175H)-CIDEA-v5 was compatible with the
166 formation of large LDs, strongly supporting the conclusion from sequence comparison
167 that positive charges are required at these positions. As histidine has a lower pKa value
168 than arginine and lysine, it can carry a positive charge depending on the pH and local
169 environment which could explain the activity retained by this protein.

170

171 **LD-LD docking is induced by the formation of CIDEA complexes.** Deletions in the
172 N-term domain of CIDEA impaired LD-LD docking, as shown by the increase in cells
173 displaying isolated LDs (Fig. 2C). Furthermore, LD clustering could be induced by
174 forcing the LD localization of the N-term fragment through conjugation with the 18-aa
175 amphipathic helix (HA-CIDEA-(1-117)-(162-180)) (Fig 3C).

176 As the N-term of CIDEA forms a highly polarized structure prone to dimerize (16), we
177 hypothesized that LD-LD docking was induced by the N-term-N-term interaction of
178 CIDEA molecules in adjacent LDs (trans complexes). However, the C-term fragment
179 (116-217) retained some degree of LD-LD docking activity (Fig 2C), indicating that an
180 additional interaction site could be present in this region. In fact, a complete blocking of
181 LD clustering was only observed with the shorter fragment 152-217, which lacks the N-
182 term and a section of the C-term (Fig. 4A).

183 The formation of CIDEA-CIDEA complexes was confirmed by co-
184 immunoprecipitation (co-IP) of CIDEA-v5 with CIDEA-HA. Surprisingly, Co-IP was
185 observed with CIDEA-(116-217)-v5 but not CIDEA-(1-118)-v5, indicating that the C-
186 term was responsible for that interaction (Fig. 4B). Interestingly, a similar percentage of
187 the input was co-IPed for constructs producing highly clustered LDs (CIDEA-
188 (R171E/R175E)-v5) and constructs showing few LD-LD contacts (CIDEA-v5 or
189 CIDEA-(116-217)-v5). Hence, this C-term interaction is largely independent of the
190 presence of LD-LD contacts, indicating that it may also occur in cis.

191 Within the C-term region, the deletion of the 162-197 sequence did not affect the
192 co-IP whereas the signal was largely reduced in CIDEA-Δ(126-155)-v5 (Fig. 4B),
193 indicating that this conserved region was involved in the C-term interaction. However,
194 the residual interaction still detectable by co-IP could sustain the LD-docking activity, as
195 cells expressing this construct displayed normal LD clustering (Fig. 4A and 4B). CIDEA-
196 (152-217)-v5 (Fig 4A and Fig. 2), which showed no LD clustering and lacks both the
197 126-155 interaction site and the N-term domain displayed a further reduction on the co-
198 IP signal (Fig 4B). Therefore, trans complexes through N-term dimerization would be
199 responsible for the LD clusters and weak co-IP signal observed in CIDEA-(126-155)-v5.
200 The lack of co-IP between the N-term fragment and the full length CIDEA could be due
201 to conformational and positional factors favouring the interaction between the HA-tagged
202 full length proteins in the LD or between the cytosolic v5-tagged N-term fragments. In
203 fact, co-IP between N-term fragments of CIDEA was previously reported (18). This
204 interaction could be disrupted with the point mutations E87Q/D88N or R55E as predicted
205 by the crystal structure of the N-term fragment which reveals the formation of
206 homodimers in which the positively charged R46, R55 and R56 in one molecule interact
207 with negative residues in the other (E87 and D88) (18). Interestingly, we found the

208 equivalent mutations in CIDEA (E79Q/D80N and R47E) impaired LD docking, while
209 R47Q and R47A, which would not create repulsions between the interacting domains did
210 not affect CIDEA activity (Fig. 2C). Taken together, these results suggest that both the
211 C-term dimerization site (126-155) and the N-term domain of CIDEA can contribute to
212 LD-LD docking by forming complexes with its counterparts on the adjacent LD.

213 **CIDEC differs from CIDEA in its dependence on the N-term domain.** The differential
214 expression of CIDEA and CIDEC in BAT and WAT could be related to the acquisition
215 of multilocular or unilocular morphologies in brown and white adipocytes (24). While
216 the ectopic expression of both CIDEA and CIDEC produce LD enlargement in a similar
217 manner, specific differences in their activity and regulation could achieve discrete
218 outcomes. In fact, whereas deletion of the N-term domain of CIDEA blocks LD
219 enlargement (Fig 2C), it has been described that the C-term fragment of CIDEC retains
220 its activity (15, 25). Here we show that similar to CIDEA, the N-term of CIDEC is
221 involved in LD-LD docking, as its deletion increases the fraction of cells displaying
222 isolated LDs (Fig. 2C). However, in the cells where the C-term of CIDEC could
223 effectively induce LD-LD docking, large LDs were observed instead of LD clusters,
224 showing that although its docking efficiency is reduced, this region of CIDEC is sufficient
225 for docking and enlarging the LDs. This differs from CIDEA, in which the C-term
226 fragment cannot induce LD enlargement despite retaining a partial LD docking activity.
227 In addition to intrinsic differences between CIDEC and CIDEA, their activity could be
228 affected by the interaction with additional proteins. While PLIN1 interacts with CIDEC,
229 but not CIDEA, and potentiates its activity (18, 26) we have observed that CIDEA
230 interacts with PLIN5 (Fig. 4D), which is enriched in BAT (27, 28). In addition to PLIN5,
231 CIDEA showed high affinity for both CIDEB and CIDEC, while it did not co-IP with
232 DFF40 or DFF45, which share homology with the N-term domain of CIDE proteins (Fig.

233 4C). As BAT cells express high levels of both CIDEA and CIDEA, the formation of CIDE
234 heterocomplexes could be involved in the regulation of LD enlargement to retain the
235 multilocular state.

236 **CIDEA interacts with Phosphatidic Acid.**

237 To further characterize the interaction of CIDEA with the LD membrane, we utilized lipid
238 strips to investigate the affinity of CIDEA for different lipids present in mammalian cell
239 membranes, finding that it selectively bound a set of anionic phospholipids (Fig. 5A). The
240 interaction with phosphatidic acid (PA) was of particular interest, as increased levels of
241 this phospholipid have been linked with LD fusion (29) and the identification of enzymes
242 such as AGPAT3 and LIPIN-1 γ in LDs supports the existence of *in situ* generation and
243 consumption of PA (13, 30). PA binding was confirmed by the strong affinity of CIDEA-
244 v5 for PA-beads (Fig. 5B), which was greatly reduced by pre-incubation of the lysate
245 with soluble PA, but not phosphatidylcholine (PC). Although the N-term fragment
246 showed some residual affinity, the main PA-binding site of CIDEA was in the C-term
247 region containing the amphipathic helix (163-180) (Fig. 5C). The charge inversion of its
248 3 cationic amino acids resulted in the loss of affinity for PA-beads in the inactive mutant
249 (K167E/R171E/R175E)-CIDEA-v5 without affecting its LD localization (Fig. 5C),
250 linking PA-binding with the TAG-transference step (Fig. 5D).

251 To investigate if PA affects the structure of the amphipathic helix, we repeated the
252 CD analyses in phosphate buffer in the presence and absence of DLPC lipid vesicles with
253 and without DLPA. Fitting of the CD data suggested a low (~5%) helical content for the
254 wild-type peptide when analysed in phosphate buffer alone, and indicated a
255 predominantly sheet / coil structure in the absence of detergent or liposomes. The
256 presence of DLPC liposomes stabilized a sharp increase in α -helical structure (up to 40%)
257 and an equivalent reduction of sheet content (Fig. 5E and Fig. 5-Figure Supplement 1),

258 yielding higher helical content than that observed in n-dodecyl- β -D-maltopyranoside
259 micelles (~25%, Fig. 3C). In contrast, the induction of helix formation by DLPC was not
260 observed in a mutant peptide carrying the substitutions impairing LD-targeting in
261 CIDEA-(F166R/V169R/L170R)-v5 (Fig. 5E). This mutant peptide remained
262 predominantly random coil in the absence and presence of DLPC liposomes.
263 Interestingly, fitting of the CD data indicated significant helical content for both the wt
264 and mutant peptides in the presence of DLPC:DLPA (9:1) vesicles (Fig. 5E and Fig. 5-
265 Figure Supplement 1). This indicates that the interaction with the negatively charged
266 phospholipid PA can compensate for the excess of positive charges in CIDEA-
267 (F166R/V169R/L170R)-v5.

268 To obtain more detailed insight into the interaction of the amphipathic helix with
269 phospholipids and the role of PA in this process, its interaction with LDs was modelled
270 by coarse-grained molecular dynamics (CG-MD) simulations (Fig. 5F-H). CG-MD
271 simulations are well established for lipid containing systems (31), including LDs (32) and
272 have the advantage over full atomistic simulations that the time scales required are much
273 smaller allowing us to compare different LD compositions and helix mutants in the large
274 multimolecular LD system. The wt (163-180) helix (CTSFKAVLRNLLRFMSYA)
275 diffused toward the LD containing 400 palmitoyl-oleoyl-glycero-phosphocholine
276 (POPC) and 200 TAG molecules where it interacted at its full length with the LD surface
277 and penetrated into the hydrophobic region of the phospholipid monolayer covering the
278 TAG core (Fig. 5F and 5G). A similar behaviour was observed by the charge inverted
279 mutant K167E/R171E/R175E (Fig. 5G and Figure. 5-Figure Supplement 2), supporting
280 the experimental result that these mutations do not affect LD localization in CIDEA (Fig.
281 2C and Fig. 3E). In contrast, no interaction with the LD was observed with the non-
282 amphipathic F166R/L169R/V169R (Fig. 5G), which also impairs LD binding in CIDEA

283 (Fig. 2C and Fig. 3E) and which was unable to attain stable secondary structure as
284 evidenced by CD (Fig. 5E). Similarly, a non-amphipathic α -helix in N-term
285 (SSLQELISKTLDVLVITT) also showed no interaction with the LD (Fig. 5G).

286 To study the effect of PA on LD structure and interaction with the CIDEA helix,
287 we replaced 10% of the PC molecules with PA. The equilibration of the system resulted
288 in a slight deformation of the spherical shape of the LD (Fig. 5-Figure supplement 2). The
289 wt helix made a stable complex with this LD at even earlier simulation times than with
290 the PC-only containing LDs (Fig. 5G and Figure 5-Figure Supplement 2). The triple-E
291 replacement mutant was also able to bind this LD, and even the F166R/L169R/V169R
292 mutant was now able to interact with the membrane (Fig. 5G). This result fits well with
293 the CD results where the addition of PA also rescued the helix induction in this mutant
294 peptide through interaction with the liposomes (Fig 5E). Interestingly, while the presence
295 of PA permitted the accommodation of the F166R/L169R/V169R helix in the LD
296 monolayer, it could not penetrate as deep toward the TAG core as the wt or helix. The
297 average distance of the peptide to the centre of the LD (\pm S.E.M.) was 5.6 ± 0.04 nm and
298 5.7 ± 0.03 nm for wt and K167E/R171E/R175E, respectively. In the presence of PA the
299 distance was 5.6 ± 0.02 nm, 5.7 ± 0.02 nm, and 6.1 ± 0.02 for wt, K167E/R171E/R175E and
300 F166R/L169R/V169R, respectively (also see Fig. 5G and 5H). This result confirms that
301 the presence of the hydrophobic face was necessary for proper helix insertion in the LD
302 monolayer.

303 The CD-MD simulations not only shed light on the interaction between the helix
304 and the LD, but also provided an indication of the mechanism by which this process could
305 lead to LD enlargement by TAG transference. We observed that TAG molecules were
306 able to escape the LD core and were integrated in the hydrophobic section of the
307 membrane (Fig. 5H). This TAG infiltration was increased after the docking of the wt helix

308 in the membrane (Fig. 5-Figure Supplement 3), suggesting that CIDEA could promote
309 the migration of TAG into the membrane as an intermediate state prior to the transference
310 to the acceptor LD. To complete the transference, the hydrophobic TAG molecules should
311 overcome the energy barrier constituted by the phospholipid polar heads and water
312 molecules in the LD-LD interface. Interestingly, we observed that the wt helix could
313 attract PA molecules in its vicinity by the interaction of its cationic residues with the
314 negatively charged polar head of PA (Fig. 5H). A direct interaction of the amphipathic
315 helix with PA was also indicated by molecular docking using Autodock Vina, which
316 supported the role of the K167, R171 and R175 residues in the interaction (Fig. 5-Figure
317 Supplement 4). Remarkably, CG-MD showed that whereas the non-amphipathic cationic
318 helix F166R/L169R/V169R also interacted with PA molecules from its superficial
319 docking position in the LD membrane, the anionic amphipathic mutant
320 K167E/R171E/R175E mutant was docked in a PA-depleted area and avoided the PA
321 molecules (Fig. 5H). Although TAG infiltration was also observed in this simulation and
322 the helix was well embedded in the membrane, its inability to attract PA molecules could
323 be responsible for the lack of TAG transference activity in CIDEA-
324 (K167E/R171E/R175E)-v5 (Fig. 5D). Taken together, these results indicate that CIDEA
325 binds the LD by embedding a cationic amphipathic helix into the LD monolayer and that
326 once there, it can interact with PA molecules, which could facilitate TAG transference.

327 We found that PA-binding was a feature common to all three members of the
328 CIDE protein family (Fig. 5C). Intriguingly, we determined that an inactive CIDEA
329 identified in a patient with lipodystrophy (33) contained a truncation (E186X), in the
330 predicted PA-binding site. Although hCIDEA-(E186X)-v5 and the equivalent mCIDEA-
331 (N172X)-v5 were localized in LDs in a high percentage of cells, they were completely
332 unable to induce LD enlargement (Fig. 5I and Fig. 2C). LD clustering activity and its

333 ability to interact with CIDE proteins was not altered in hCIDEA-(E186X)-v5 (Fig 5I and
334 5J), but it showed no affinity for PA (Fig. 5K). Thus, PA-binding could be involved in
335 the lipid transfer phase of CIDE activity.

336 **PA is required for LD enlargement.**

337 To confirm the requirement of PA binding, we examined the effect of PA
338 depletion on CIDEA activity. While substantial alterations in the phospholipid
339 composition of mammalian cells often compromise their viability, yeast cells offer a wide
340 range of genetically modified strains with well characterized alterations in phospholipid
341 metabolism (Fig. 6A) (34). Thus, despite the absence of CIDE homologues in yeast (35),
342 we explored the functionality of CIDEA in wild type and genetically modified strains of
343 *S. cerevisiae* (Fig. 6-Figure Supplement 1).

344 Murine CIDEA could be stably expressed in yeast cells (Fig. 6B), producing an
345 increase in the size of their LDs (Fig. 6C). Yeast cells expressing wt CIDEA, but not the
346 inactive R171E/R175E mutant, contained fewer and larger LDs than the control (Fig. 6D-
347 F), indicating that murine CIDEA was functional in these cells. By measuring the
348 frequency of supersized LDs (diameter above 0.5 μ m) and the total number of LDs in
349 strains with altered lipid metabolism we could determine in which yeast strains CIDEA
350 was able to induce LD enlargement (Fig. 6E-F). CIDEA was inactive in cells defective in
351 phospholipase D (*pld1* Δ) (36), which catalyzes the production of PA from PC. CIDEA
352 activity was also abrogated in cells expressing a hyperactive form of the PA
353 phosphohydrolase (PAH1-7A) (37, 38). These results indicate that PA is necessary for
354 CIDEA activity. In addition, we observed that total cellular PA levels were increased by
355 CIDEA, an effect that was prevented by the expression of PAH1-7A (Fig. 6G). As the
356 PA synthesis rate was not affected (Fig. 6H), CIDEA could be protecting a pool of PA
357 from degradation.

358 The deletion of diacylglycerol kinase (*dgk1Δ*) (39), did not affect CIDEA activity. *DGK1*
359 is important for the generation of phospholipids from TAG as cells exit from stasis (40),
360 but its deletion has not been shown to have a great effect on PA levels under normal
361 growth conditions. Regarding *PAH1*, its deletion produces dramatic cellular effects (41),
362 including defective LD formation (42, 43). As this alteration in LDs can be compensated
363 by the deletion of *DGK1*, we chose to use the *dgk1Δpah1Δ* strain, observing normal LD
364 enlargement by CIDEA (Fig. 6E-F). CIDEA was also able to further increase the LD size
365 in the *cho2Δ* strain, which lacks the phosphatidylethanolamine (PE) methylation pathway
366 for PC synthesis, and has been shown to present supersized LDs and high levels of PA
367 and PE (29). The CIDEA-induced LD enlargement in yeast was not due to a mere coating
368 effect protecting LDs against lipases, as it was functional in the *tgl3Δtgl4Δtgl5Δ* strain,
369 which lacks lipase activity. As expected, CIDEA could not induce the appearance of LDs
370 in *dga1Δlro1Δare1Δare2Δ* cells (Fig. 6D), which are deficient in the enzymes required
371 for TAG and steryl ester synthesis and contain no LDs (44).

372 To study the role of PA-dependent CIDEA action in mammalian cells without
373 compromising other PA-dependent cellular processes, we specifically degraded this
374 phospholipid in LDs by overexpressing a LD-localized isoform of PA phosphohydrolase
375 (LIPIN-1 γ) (30, 45). While CIDEA-HA displayed normal activity in cells co-transfected
376 with an empty vector, it was unable to promote LD enlargement in cells expressing
377 LIPIN-1 γ -v5 (Fig. 6I-J). LIPIN-1 γ -v5 showed affinity for PA but it did not coIP with
378 CIDEA, indicating that its inhibitory effects were not due to a direct interaction between
379 these proteins (Fig. 6K-L). Taken together, these results reveal that the mechanism of
380 action of CIDEA involves direct interaction with PA molecules in the LD monolayer.

381 Discussion

382 The Cidea gene is highly expressed in BAT, induced in WAT following cold
383 exposure (46), and is widely used by researchers as a defining marker to discriminate
384 brown or brite adipocytes from white adipocytes (7, 28). As evidence indicated a key role
385 in the LD biology (47) we have characterized the mechanism by which CIDEA promotes
386 LD enlargement, which involves the targeting of LDs, the docking of LD pairs and the
387 transference of lipids between them. The lipid transfer step requires the interaction of
388 CIDEA and PA through a cationic amphipathic helix. Independently of PA-binding, this
389 helix is also responsible for anchoring CIDEA in the LD membrane. Finally, we
390 demonstrate that the docking of LD pairs is driven by the formation of CIDEA complexes
391 involving the N-term domain and a C-term interaction site.

392 CIDE proteins appeared during vertebrate evolution by the combination of an
393 ancestor N-term domain and a LD-binding C-term domain (35). In spite of this, the full
394 process of LD enlargement can be induced in yeast by the sole exogenous expression of
395 CIDEA, indicating that in contrast to SNARE-triggered vesicle fusion, LD fusion by lipid
396 transference does not require the coordination of multiple specific proteins (48). Whereas
397 vesicle fusion implicates an intricate restructuring of the phospholipid bilayers, LD fusion
398 is a spontaneous process that the cell has to prevent by tightly controlling their
399 phospholipid composition (23). However, although phospholipid-modifying enzymes
400 have been linked with the biogenesis of LDs (49, 50), the implication of phospholipids in
401 physiologic LD fusion processes has not been previously described.

402 Complete LD fusion by lipid transfer can last several hours, during which the
403 participating LDs remain in contact. Our results indicate that both the N-term domain and
404 a C-term dimerization site (aa 126-155) independently participate in the docking of LD
405 pairs by forming trans interactions (Fig. 7). Certain mutations in the dimerization sites
406 that do not eliminate the interaction result in a decrease on the TAG transference

407 efficiency, reflected on the presence of small LDs docked to enlarged LDs. This suggests
408 that in addition to stabilizing the LD-LD interaction, the correct conformation of the
409 CIDEA complexes is necessary for optimal TAG transfer. Furthermore, the formation of
410 stable LD pairs is not sufficient to trigger LD fusion by lipid transfer. In fact, although
411 LDs can be tightly packed in cultured adipocytes, no TAG transference across neighbour
412 LDs is observed in the absence of CIDE proteins (15), showing that the phospholipid
413 monolayer acts as a barrier impermeable to TAG. Our CG-MD simulations indicate that
414 certain TAG molecules can escape the neutral lipid core of the LD and be integrated
415 within the aliphatic chains of the phospholipid monolayer. This could be a transition state
416 prior to the TAG transference and our data indicates that the docking of the amphipathic
417 helix in the LD membrane could facilitate this process. However, the infiltrated TAGs in
418 LD membranes in the presence of mutant helices, or even in the absence of docking,
419 suggests that this is not enough to complete the TAG transference.

420 To be transferred to the adjacent LD, the TAGs integrated in the hydrophobic
421 region of the LD membrane should cross the energy barrier defined by the phospholipid
422 polar heads, and the interaction of CIDEA with PA could play a role in this process, as
423 suggested by the disruption of LD enlargement by the mutations preventing PA-binding
424 (K167E/R171E/R175E) and the inhibition of CIDEA after PA depletion. The minor
425 effects observed with more conservative substitutions in the helix, suggests that the
426 presence of positive charges is sufficient to induce TAG transference by attracting anionic
427 phospholipids present in the LD membrane. PA, which requirement is indicated by our
428 PA-depletion experiments, is a cone-shaped anionic phospholipid which could locally
429 destabilize the LD monolayer by favoring a negative membrane curvature incompatible
430 with the spherical LD morphology (51). Interestingly, while the zwitterion PC, the main
431 component of the monolayer, stabilizes the LD structure (23), the negatively charged PA

432 promote their coalescence (29). This is supported by our CD-MD results which resulted
433 in a deformation of the LD shape by the addition of PA. We propose a model in which
434 the C-term amphipathic helix positions itself in the LD monolayer and interacts with PA
435 molecules in its vicinity, which might include trans interactions with PA in the adjacent
436 LD. The interaction with PA disturbs the integrity of the phospholipid barrier at the LD-
437 LD interface, allowing the LD to LD transference of TAG molecules integrated in the LD
438 membrane (Fig. 7). Additional alterations in the LD composition could be facilitating
439 TAG transference, as differentiating adipocytes experience a reduction in saturated fatty
440 acids in the LD phospholipids (52), and in their PC/PE ratio (53) which could increase
441 the permeability of the LD membranes, and we previously observed that a change in the
442 molecular structures of TAG results in an altered migration pattern to the LD surface (32).

443 During LD fusion by lipid transfer, the pressure gradient experienced by LDs
444 favors TAG flux from small to large LDs (15). However, the implication of PA, a minor
445 component of the LD membrane, could represent a control mechanism, as it is plausible
446 that the cell could actively influence the TAG flux direction by differently regulating the
447 levels of PA in large and small LDs, which could be controlled by the activity of enzymes
448 such as AGPAT3 and LIPIN-1 γ (13, 30). This is a remarkable possibility, as a switch in
449 the favored TAG flux direction could promote the acquisition of a multilocular phenotype
450 and facilitate the browning of WAT (24). Interestingly, Cidea mRNA is the LD protein-
451 encoding transcript that experiences the greatest increase during the cold-induced process
452 by which multilocular BAT-like cells appear in WAT (24). Furthermore, in BAT, cold
453 exposure instigates a profound increase in CIDEA protein levels that is independent of
454 transcriptional regulation (54). The profound increase in CIDEA is coincident with
455 elevated lipolysis and de novo lipogenesis that occurs in both brown and white adipose
456 tissues after β -adrenergic receptor activation (55). It is likely that CIDEA has a central

457 role in coupling these processes to package newly synthesized TAG in LDs for
458 subsequent lipolysis and fatty acid oxidation. Importantly, BAT displays high levels of
459 glycerol kinase activity (56, 57) that facilitates glycerol recycling rather than release into
460 the blood stream, following induction of lipolysis (58), which occurs in WAT. Hence, the
461 reported elevated glycerol released from cells depleted of CIDEA (28) is likely to be a
462 result of decoupling lipolysis from the ability to efficiently store the products of
463 lipogenesis in LDs and therefore producing a net increase in detected extracellular
464 glycerol. This important role of CIDEA is supported by the marked depletion of TAG in
465 the BAT of Cidea null mice following overnight exposure to 4 °C (28) and our findings
466 that CIDEA-dependent LD enlargement is maintained in a lipase negative yeast strain.

467 Cidea and the genes that are required to facilitate high rates of lipolysis and
468 lipogenesis are associated with the “browning” of white fat either following cold exposure
469 (46) or in genetic models such as RIP140 knockout WAT (59). The induction of a brown-
470 like phenotype in WAT has potential benefits in the treatment and prevention of metabolic
471 disorders (60). Differences in the activity and regulation of CIDEC and CIDEA could
472 also be responsible for the adoption of unilocular or multilocular phenotypes. In addition
473 to their differential interaction with PLIN1 and 5, we have observed that CIDEC is more
474 resilient to the deletion of the N-term than CIDEA, indicating that it may be less sensitive
475 to regulatory posttranslational modifications of this domain. This robustness of CIDEC
476 activity together with its potentiation by PLIN1, could facilitate the continuity of the LD
477 enlargement in white adipocytes until the unilocular phenotype is achieved. In contrast,
478 in brown adipocytes expressing CIDEA the process would be stopped at the multilocular
479 stage for example due to post-translational modifications that modulate the function or
480 stability of the protein or alteration of the PA levels in LDs.

481 Further work will be required to characterize the physiological differences
482 between CIDEc and CIDEA and determine the influence of their interacting partners and
483 the role of proteins able to alter the LD PA levels, such as Lipin-1 γ . Abnormal
484 accumulation of large LDs have also been observed in non-adipocyte cells under other
485 pathological conditions such as liver steatosis and atherosclerosis (61). As enhanced
486 expression of CIDE proteins have been linked to these conditions (62-64), the modulation
487 of CIDE-triggered LD enlargement represents a potential therapeutic strategy which
488 requires the elucidation of its molecular mechanism.

489 In summary, we found that during LD fusion by lipid transference, CIDEA
490 ensures the close proximity of the LD membranes by forming trans complexes through
491 its N-term and its C-term dimerization sites. This protein complex will be anchored in the
492 LD-LD interface, forming the molecular environment necessary for TAG transport across
493 the membrane. Finally, the amphipathic helix embedded in the LD membrane, interacts
494 with the cone-shaped phospholipid PA, generating a local perturbation of the monolayer
495 integrity that would increase its permeability to TAG and enable its exportation to the
496 acceptor LD. The new mechanistic insight into the molecular events underpinning LD
497 dynamics revealed by this study highlight CIDEA and PA production as targets for
498 therapeutic modulation of LD accumulation.

499

500 **Acknowledgements**

501 We thank Dr. Carole Sztalryd for providing the Plin expression vectors, Dr. David Savage
502 for the hCIDEc constructs, and Prof Parmjit Jat for providing retrovirus to express the
503 temperature-sensitive SV40 large T antigen. We are also grateful to Dr. Vishwajeet Puri
504 for critical reading of the manuscript. This work was supported by the BBSRC grant
505 BB/H020233/1, the EU FP7 project DIABAT (HEALTH-F2-2011-278373), the Genesis

506 Research Trust and by National Institutes of Health grants GM- 19629 (to S.A.H.) and
507 GM-28140 (to G.M.C.)
508

509 **Materials and Methods**

510 **Plasmids and antibodies.** The coding region of murine Cidea, Cideb, Cidec, Dff40 and
511 Dff45 were cloned into the vector pcDNA3.1D/V5-His-TOPO (Invitrogen) to obtain the
512 v5-tagged versions of the proteins (47). The human full length and truncated forms of
513 Cidec were subcloned into pcDNA3.1D/V5-His-TOPO from their GFP constructs (33)
514 and Lipin-1 γ -v5 was constructed from pGH321 (45). Mutations and deletions were
515 generated with the QuikChange Lightning Kit (Agilent). Tagged proteins were detected
516 by using antibodies against v5 (Invitrogen, R96025), HA (Sigma, H6908) or GFP
517 (Abcam, ab1218).

518 **Cell culture and transfection.** 3T3-L1 cells were maintained in Dulbecco's modified
519 Eagle's medium (DMEM) containing 4.5 g/l glucose and L-glutamine supplemented with
520 10% newborn calf serum (NCS, Invitrogen) and penicillin/streptomycin at 37 °C and 5%
521 CO₂. Hela cells were cultured in similar conditions but with 10% FBS (Invitrogen).
522 Transfections were performed using Lipofectamine 2000 (Invitrogen). Stable cell lines
523 expressing CIDEA-v5 were generated by transfection of 3T3-L1 cells with
524 pcDNA3.1/Cidea-v5 followed by selection with G418 (Invitrogen). The imBAT cell line
525 was generated by the retroviral transduction of primary brown adipocytes with SV40
526 large-T antigen tsA58 mutant and differentiated as previously described (47).

527 **4D live cell imaging.** Cells in gelatin-coated glass-bottom dishes were stained with 0.1-
528 0.5 μ g/ml BODIPY 493/503 in the appropriate culture medium with 20 mM HEPES in
529 the absence of serum. After 10 minutes at 37 °C, 10% FBS was restored and the dish was
530 equilibrated at 37 °C in a Leica SP5 confocal microscope. Time-lapse Z-stacks were
531 acquired every 2 minutes, and represented as their maximum projection. 3T3-L1 cells
532 were analysed 6 hours after infection with an adenovirus vector expressing CIDEA (47).
533 For the imBAT differentiation experiments, preadipocytes were incubated for 48 hours

534 with differentiation cocktail (47), and medium was changed to DMEM:F12 with 10%
535 FBS, 1nM T3 and 170 nM insulin for 6 hours before staining.

536 **Immunofluorescence.** Cells on glass coverslips were fixed in 4% paraformaldehyde, and
537 permeabilized with blocking solution (BS: 0.5% BSA, 0.05% Saponin, 50 mM NH₄Cl,
538 in PBS). Cells were incubated overnight at 4 °C with primary antibodies diluted in BS,
539 and for 1 hour at room temperature with secondary antibodies (conjugated to Alexa488
540 and Alexa555, Invitrogen). Cells were stained in PBS with 2 µg/ml BODIPY 493/503 or
541 1:200 dilution of LipidToxTM Deep Red for 15 minutes and mounted in ProLong® Gold
542 antifade reagent (all from Invitrogen). Images were acquired in a Leica TCS SP5
543 microscope. For the phenotypic distribution of Hela cells expressing modified CIDEA–
544 v5 constructs, cells were treated with oleic acid 24 hours after transfection and incubated
545 for further 18 hours prior to fixation. Phenotype classification was performed by visual
546 analysis of randomized samples in a minimum of three independent experiments for each
547 construct (n > 50 cells)

548 **Liposome Preparation.** Liposomes were prepared by dissolving lipid (1,2-dilauroyl-sn-
549 glycerol-3-phosphocholine (DLPC, 12:0 PC) or a mixture of DLPC and DLPA (1,2-
550 dilauroyl-sn-glycerol-3-phosphate, 12:0 PA) at a 9:1 DLPC:DLPA molar ratio) (Echelon
551 Biosciences Inc., USA) in 3:1 chloroform:MeOH and drying under vacuum using rotary
552 evaporation. The resulting thin films were left to dry under vacuum overnight to remove
553 all residual solvent, reconstituted in 25 mM sodium phosphate buffer (pH 7.2) to a final
554 lipid concentration of 3.3 mg/mL, and subjected to 4 times freeze-thaw-sonicate cycles.
555 The vesicles were incubated at 37°C for 20 minutes prior to CD measurements.

556 **Circular dichroism.** CD experiments were undertaken with a synthetic wild type
557 (SYDIRCTSFKAVLRNLLRFMSYAAQMTG) CIDEA peptide (Pepmic Co, Ltd,
558 Suzhou, China) encompassing aas 158-185 solubilized at a concentration of 41µM (based

559 on absorbance at 280nm) in 50 mM Potassium phosphate, pH 6.2 plus 0.1% n-dodecyl-
560 β -D-maltopyranoside and analysed by circular dichroism (CD) in a JASCO J-815
561 spectrometer.

562 Additional CD experiments with the same wt peptide and a mutant
563 (F166R/V169R/L170R) (SYDIRCTSRKARRRNLLRFMSYAAQMTG) were carried
564 out using a Jasco J-1500 spectropolarimeter (Jasco UK, Great Dunmow, UK) equipped
565 with a Peltier thermally controlled cuvette holder and 1 mm path-length quartz cuvettes
566 (Starna, Optiglass Ltd, Hainault, UK). Spectra were recorded between 190-300 nm with
567 a data pitch of 0.2 nm, a bandwidth of 2 nm, a scanning speed of 100 nm min⁻¹ and a
568 response time of 1 second. Peptides were solubilized in 25 mM sodium phosphate (pH
569 7.2) at concentrations of 70 μ M (wt) and 47 μ M (mutant). Peptide samples were prepared
570 in the absence and presence of DPLC and DLPC:DLPA (9:1 molar ratio) vesicles and CD
571 spectra were acquired at 37°C. Data shown were averaged from four individual spectra
572 after subtraction of the appropriate buffer/vesicle CD spectrum. All CD data was analysed
573 using the CDPro suite of programs. The output of the individual programs CDSSTR and
574 CONTINLL provided the estimated percentages of α -helix, β -sheet, turn and
575 unstructured regions, using the IB=4 database of 43 soluble proteins with CD data from
576 190 to 250 nm.

577 **Structure Prediction and Molecular Docking.** Secondary structure propensity of full-
578 length CIDEA was predicted using DSSP (65). The amphipathic helix sequence
579 CTSFKAVLRNLLRFMSYA (163-180 aa) was submitted to the PEP-FOLD online de
580 novo peptide structure prediction server using default settings (66). Phosphatidic acid
581 (PA) was docked to the PEP-FOLD predicted structure using default settings in a single
582 simulation by AutoDock Vina53 (<http://vina.scripps.edu>) (67). Lipid and protein
583 structures were converted from pdb into pdbqt format using MGL Tools54. A grid box

584 was centred at coordinates 35.651, 35.471, 35.569 with 34Å units in x, y and z directions
585 to cover the entire helix. AutoDock Vina reports the 9 lowest energy conformations,
586 which were inspected using PyMOL software (www.pymol.org). According to binding
587 affinity and visual inspection, without RMSD clustering, the best-fit model has been
588 selected.

589 **Coarse Grained Molecular Dynamics (CG-MD) simulations.** Coarse grained (CG)
590 molecular dynamics (MD) simulations were used to predict the structure of a lipid droplet
591 (LD) and its putative interaction with the amphipathic helix using a 4 to 1 atom mapping
592 for both, lipids and protein (31, 68). A LD composed of a hydrophobic core containing
593 200 glyceryl trioleate or triacylglycerol (TAG) molecules surrounded by a phospholipid
594 monolayer containing 400 palmitoyl-oleoyl-glycero-phosphocholine (POPC) molecules
595 previously reported was used as the starting configuration (32). A second LD containing
596 PA consisting of a hydrophobic core of 200 TAG molecules, and a phospholipid
597 monolayer with 364 POPC molecules and 36 palmitoyl-oleoyl-glycero-phosphatidic acid
598 (POPA) was compiled using the same procedure. A rectangular simulation box including
599 LD, amphipathic helix, water and ions was energy minimized and pre-equilibrated. All
600 MD runs were carried out for 200ns under NPT conditions. The CG-MD simulation of
601 the LD-helix interaction was carried out using the MARTINI CG force field developed
602 by Marrink et al. (version 2.0) (31). All simulations were performed using the
603 GROMACS simulation package version 4.6.5 (<http://www.gromacs.org/>). The system
604 was weakly coupled to an external temperature bath at 310 K (69). The pressure was
605 weakly coupled to an external bath at 1 bar using an isotropic pressure scheme (69).
606 Visualization and analysis was performed using the VMD v.1.9 visualization software
607 (70). Distances and density maps were computed using analysis tools (`g_dist` and
608 `g_densmap`) in the GROMACS package (<http://www.gromacs.org>) (71).

609 **Immunoprecipitation (IP).** Cells were lysed in 50 mM Tris (pH 8.0), 150 mM NaCl,
610 1% TRITON X-100 with protease inhibitor cocktail (Roche). Anti-HA antibody (H6908;
611 Sigma) or anti-V5 antibody (R96025; Invitrogen) was bound to Dynabeads Protein G
612 (Invitrogen) and incubated with the lysate to IP the tagged proteins following
613 manufacturer's instructions. Cell lysates or IP fractions in Laemmli buffer were analysed
614 by Western blot. Each co-IP experiment was performed at least in triplicate, producing
615 similar results in each experiment with a representative image presented.

616 **Lipid binding assays.** In vitro translated CIDEA-v5 was synthesized from
617 pcDNA3.1/Cidea-v5 using the TnT® Coupled Wheat Germ Extract System (Promega),
618 and verified by Western blot. The cell-free preparation of CIDEA-v5 was probed with
619 Membrane Lipid Strips™ (Echelon) following the manufacturer's instructions. Protein
620 affinity for PA was examined in pull-down assays using PA covalently linked to agarose
621 beads (PA-beads) (72). Cells were lysed in 50 mM Tris-HCl pH 8.0, 50 mM KCl, 10 mM
622 EDTA, 0.5% Nonidet P-40 and protease inhibitors. Lysates were sonicated and
623 centrifuged at 14000g prior to incubation with the PA beads as previously described (72).
624 Competition experiments with soluble phospholipids were performed by supplementing
625 the cell lysate with 1,2-dilauroyl-sn-glycero-3-phosphate 12:0 PC (DLPA) or 1,2-
626 dilauroyl-sn-glycero-3-phosphocholine (DLPC) (Echelon). Each PA-binding experiment
627 was performed at least in triplicate, producing similar results in each experiment with a
628 representative image presented.

629 **CIDEA expression in yeast.** The *S. cerevisiae* strains used in this study are listed in
630 Supplemental File 1. To express CIDEA in yeast, a codon-optimized version of the mouse
631 Cidea gene was generated by artificial gene synthesis (GeneOracle), and subcloned into
632 pRS316-CYC1p. Wild type BY4742 (73) and genetically modified yeast strains were
633 transformed with pRS316-CYC1p-Cidea and stable transformants were selected in

634 synthetic media minus uracil. Leucine selection was used for the expression of PAH1-7A
635 with pH204 (37).

636 **Microscopy analysis of yeast lipid droplets and image processing.** Yeast cells in
637 synthetic media cultured overnight at 30 °C were diluted to OD₆₀₀=0.1 and allowed to
638 grow until mid-logarithmic phase (OD₆₀₀=0.5) before fixation with 4% formaldehyde
639 and LD staining with 2 µg/ml BODIPY 493/503. For the automatic quantification of LDs,
640 random microscopy images were acquired using a Delta Vision RT system (Applied
641 Precision). Maximum intensity and integrated intensity projections were created from the
642 deconvolved image stacks using ImageJ. A custom written CellProfiler pipeline (74)
643 automatically identified individual yeast cells and measured their number and size of
644 circle shaped LDs. Supersized LDs were defined as the LDs with a diameter above 0.5
645 µm.

646 **Steady state and pulse labeling of phospholipids.** To measure the total levels of
647 phospholipids in yeast, cells were grown overnight in synthetic medium at 30 °C in the
648 presence of 20 µCi/mL [³²P]-orthophosphate. Cultures were then diluted to OD₆₀₀=0.1
649 maintaining the label and were allowed to grow until OD₆₀₀=0.5. To analyse *de novo*
650 synthesis of glycerophospholipids, cells were grown to OD₆₀₀=0.5 in synthetic medium
651 and incubated with 100 µCi/mL [32P]-for 20 min. Lipids were extracted and quantified
652 by two-dimensional chromatography, as described by Gaspar et al (75).

653

654 **FIGURE Legends**

655 **Figure 1. CIDEA promotes LD enlargement by transference of lipids.** (A) Live
656 imaging of the LD dynamics during the differentiation of a brown preadipocyte, showing
657 the characteristic CIDE-triggered LD enlargement, characterized by the progressive
658 transference of lipids from a donor to an acceptor LD until it is completely absorbed. (B)
659 Live imaging of the LD dynamics in an undifferentiated 3T3-L1 cell 6 hours after
660 infection with adenoviral particles carrying the CIDEA gene. Red arrows highlight the
661 transient formation of irregularly shaped LD clusters, while yellow arrows mark the
662 fusion of two droplets by transference of lipids. (C) CIDEA-v5 expression in Hela cells
663 induces LD enlargement. An enrichment in CIDEA-v5 (red) can be observed in the
664 contact site between two LDs (green). (D) Detail of LD fusion by slow transference of
665 lipids in a 3T3-L1 cell stably expressing CIDEA-v5.

666 **Figure 2. Mapping the functional domains of CIDEA.** (A) Amino acid sequence of
667 murine CIDEA, highlighting the residues conserved in either CIDEB or CIDEA (grey
668 underline) or in both proteins (black underline). The substituted aa in mutant constructs
669 appear in red, and a positively charged sequence necessary for the TAG transfer step is
670 encircled in orange. Four highly conserved regions are defined and symbolized by colour
671 boxes in a linear representation of CIDEA-v5. The theoretical isoelectric point of each
672 fragment is indicated inside the boxes. (B) Representative images of the different
673 phenotypes observed in Hela cells overexpressing mutated forms of CIDEA-v5. 24 hours
674 after transfection cells were treated with oleic acid and incubated for further 18 hours
675 prior to fixation. Cells were classified into 6 major phenotypes. Cells expressing fully-
676 active forms of CIDEA had few and large LDs (Type I). In some mutants, the large LDs
677 remained attached to many small LDs, indicating that lipid transfer was inefficient or
678 inactive for some LDs (Type II). When CIDEA alterations blocked the lipid transfer

679 process, the LDs remained small and grouped in a few large clusters (Type III). If this
680 was accompanied by inefficient LD-LD docking, the cells contained a number of small
681 LD clusters combined with isolated LDs (Type IV). The CIDEA forms which could not
682 stabilize LD-LD interactions displayed a phenotype similar to the mock transfected cells,
683 with most of the LDs dispersed thorough the cytoplasm (Type V). Finally, some CIDEA
684 constructs were unable to target the LDs, indicating an alteration of the LD-binding
685 domain (Type VI). (C) Morphologic distribution of cells expressing each of the studied
686 CIDE constructs. The phenotypic distribution was performed in a minimum of three
687 independent experiments for every construct (n > 50 cells).

688

689 **Figure 2 – Figure Supplement 1. Alignment of amino acid sequences of CIDEA,**
690 **CIDEB and CIDEC.** Clustal format alignment of murine CIDEA, CIDEB and CIDEC,
691 performed using T-COFFEE (www.tcoffee.org). Amino acid sequences were obtained
692 from <http://ensembl.org>. "*" means residues are identical in all sequences in the
693 alignment, ":" means conserved substitutions have been observed, "." means that semi-
694 conserved substitutions are observed. Four highly conserved regions are defined by
695 colour boxes.

696 **Figure 3. CIDEA targets the LD monolayer through a cationic amphipathic helix.**
697 (A) Secondary structure of CIDEA predicted by SWISS-MODEL server. (B) Helical
698 wheel representation of the putative amphipathic α -helix (163–180) generated at
699 <http://heliquest.ipmc.cnrs.fr/>. (C) Circular Dichroism spectra of a 28-aa peptide
700 corresponding to the 158-185 sequence of CIDEA (200 μ M) solubilized in 50 mM
701 Potassium phosphate, pH 6.2 plus 0.1% n-dodecyl- β -D-maltopyranoside. (D) A Hela cell
702 expressing HA-CIDEA-(1-120)-v5 (red) or HA-CIDEA-(1-117)-(163-180) (red),

703 showing the inclusion of aas 163-180 enhances LD localization and the ability to promote
704 LD docking. The phenotypic distribution was performed in a minimum of three
705 independent experiments for every construct (n > 50 cells). **(E)** A HeLa cell expressing
706 CIDEA-(F166R/V169R/L170R)-v5 (red) showing amino acid substitutions to
707 compromise amphipathicity of the helix disrupt LD targeting, and a HeLa cell expressing
708 CIDEA-(K167E/R171E/R175E)-v5 (red), showing amino acid substitutions to invert the
709 charge of the helix but maintaining amphipathicity retains predominantly LD localization.

710 **Figure 3-Figure supplement 1. Conservation of amino acids for CIDEA amphipathic**
711 **helix across vertebrate species.** A) Alignment of amino acid sequences for CIDEA over
712 a range of vertebrate species corresponding to the amphipathic α -helix (aas 163–180 of
713 murine). Amino acid sequences were obtained from <http://ensembl.org> and initially
714 aligned using WebPRANK at <http://ebi.ac.uk>. Sequences were then grouped based on
715 species phylogeny. (B) Helical wheel representation of the CIDEA putative amphipathic
716 α -helix for indicated species (corresponding to murine aas 163–180) generated at
717 <http://heliquist.ipmc.cnrs.fr/>.

718 **Figure 4. LD-LD docking and CIDEA interactions.** (A) A HeLa cell expressing
719 CIDEA-(152-217)-v5, showing normal recruitment to LDs, but no LD docking. A HeLa
720 cell expressing CIDEA- Δ (126-155)-v5, showing normal LD-LD docking but inefficient
721 LD enlargement as revealed by the presence of clusters of small and large LDs.
722 Representative images are shown of experiments performed in a minimum of three
723 independent experiments for every construct (n > 50 cells). **(B)** Co-IP assays between
724 CIDEA-HA and different CIDEA-v5 constructs. The observed CIDEA-CIDEA
725 interaction was driven by the C-term domain and required the presence of the 126-155 aa
726 sequence. **(C-D)** Co-IP assays showing CIDEA interactions with CIDEB, CIDEA and

727 PLIN5. Each co-IP was performed at least in triplicate, producing similar results in each
728 experiment.

729 **Figure 5. CIDEA is a PA binding protein.** (A) Lipid strip assay showing the affinity of
730 CIDEA-v5 for certain anionic phospholipids. (B) Interaction of CIDEA-v5 with PA-
731 beads. Binding was reduced by pre-incubation of the lysate with soluble PA, but not PC.
732 (C) The affinity for PA-beads was highly reduced in CIDEA-v5 constructs with
733 alterations in its C-term hydrophobic and basic region (162-197). (D) CIDEA-
734 (K167E/R171E/R175E)-v5 localizes to LDs and induces their clustering but cannot
735 promote their enlargement by lipid transfer. Representative images are show of
736 experiments performed in a minimum of three independent experiments for every
737 construct (n > 50 cells). (H) Circular Dichroism spectra of the synthetic wild type (wt) or
738 mutant (F166R/V169R/L170R) CIDEA peptides encompassing aas 158-185 solubilized
739 in 25 mM sodium phosphate (pH 7.2) at a concentrations of 70 μ M (wt) and 47 μ M
740 (mutant). Peptide samples were prepared in the absence and presence of increasing
741 amounts of DPLC or DLPC:DLPA (9:1 molar ratio). (F-H) CG-MD simulations of
742 peptide interactions with LDs (PC: hydrophobic chains, transparent blue, polar heads,
743 opaque blue; TAG: hydrophobic chains, dark brown, glycerol chain, light brown; PA:
744 hydrophobic chains, transparent red, polar heads, opaque red; peptides: yellow, with
745 cationic aa in blue and anionic in red). (F) Selected time points of the wt helix simulation
746 with PC-LDs. At 124 the helix initiates the contact through its hydrophobic face, being
747 rapidly embedded in the phospholipid monolayer. TAG molecules can abandon the
748 neutral lipid core and are integrated in the hydrophobic region of the phospholipid
749 monolayer. (G) Distance between the peptide and LD centre of mass (COM) vs time for
750 the different helices with a PC-LD and a PC:PA-LD. The dashed line represents the
751 approximate location of LD phospholipid head groups. (H) Different views of the

752 configuration of the LD-helix at the end of the simulations. Interaction between the polar
753 head of PA and the helix can be observed for the wt and F166R/V169R/L170R but not
754 K167E/R171E/R175E. **(I-K)** Comparison of full length hCIDEA-v5 and the
755 lipodystrophy-associated truncation hCIDEA-(E186X)-v5, including LD localization and
756 morphology **(I)**, co-IP with CIDEA-HA **(J)** and affinity for PA-beads **(K)**. Each co-IP,
757 PA-binding assay and Lipid strip assay was performed at least in triplicate, producing
758 similar results in each experiment.

759 **Figure 5-Figure Supplement 1. Secondary structure determination of CIDEA amino**
760 **acids 158-185 (wild type and F166R/V169R/L170R) by CDPro DATABASE 4 (43**
761 **soluble proteins) using the CONTINLL program.**

762

763 **Figure 5-Figure Supplement 2. Computational prediction of the amphipathic helix**
764 **and LD interactions. (A)** CG-MD simulations of peptide interactions with LDs (PC:
765 hydrophobic chains, transparent blue, polar heads, opaque blue; TAG: hydrophobic
766 chains, dark brown, glycerol chain, light brown; PA: hydrophobic chains, transparent red,
767 polar heads, opaque red; peptides: yellow, with cationic aa in blue and anionic in red).
768 Selected time points of the wt helix and K167E/R171E/R175E helix simulation with PC-
769 LDs or PC:PA-LDs are indicated.

770 **Figure 5-Figure Supplement 3. TAG infiltration into the phospholipid monolayer.**

771 **(A)** 2D number density maps of TAG molecules along the z direction from the CG-MD
772 simulations. TAG frequency was measured over 76 ns before and after the docking of the
773 wt helix to the membrane. The differential distribution before and after docking reveals
774 an increase on the presence of TAG molecules in the membrane, revealed by the red spots
775 in the outer arch and blue in the inner.

776 **(B)** CG-MD simulations of peptide interactions with LDs (PC: hydrophobic chains,
777 transparent blue, polar heads, opaque blue; TAG: hydrophobic chains, dark brown,
778 glycerol chain, light brown; PA: hydrophobic chains, transparent red, polar heads, opaque
779 red; peptides: yellow, with cationic aa in blue and anionic in red). Selected time points of
780 the wt helix with PC-LD show TAG molecules in the LD membrane were increased after
781 CIDEA peptide docking (170ns vs 24ns).

782 **Figure 5-Supplemental figure 4. Computational prediction of PA docking to the**
783 **amphipathic helix structure of CIDEA. (A)** Charge-smoothed potential of the predicted
784 putative amphipathic helix of murine CIDEA (aas 163-180). Stick representation has been
785 employed to highlight the positively charged residues K167, R171 and R175. **(B)** The
786 nine top-ranked models from molecular docking of PA and the amphipathic helix using
787 Autodock Vina. Interaction of the PA phosphate group with R171 and R175 is observed
788 in eight of them, while the hydrophobic chains of the phospholipid can adopt multiple
789 configurations.

790 **Figure 6. CIDEA is functional in yeast and requires PA. (A)** Pathway showing the
791 reactions catalyzed by the enzymes altered in the studied yeast strains. **(B)** Stable
792 expression of mCIDEA-v5 in three transformed yeast clones. **(C)** Frequency distribution
793 of the diameter of the largest LD per cell. **(D)** LD staining in the studied yeast strains
794 transformed with pRS316-CYC1p-Cidea or the empty vector. **(E-F)** Quantification of LD
795 size and number per cell in randomly acquired images (100-200 cells/condition). CIDEA
796 activity in yeast was measured by its ability to increase the percentage of cells with
797 supersized LDs **(E)** and reduce the total number of LDs per cell **(F)**. **(G-H)** Effect of
798 CIDEA and *PAH1-7A* expression in the cellular levels of PA **(G)** and its synthesis rate
799 **(H)**. Three different yeast clones per condition were analysed, and results are shown as

800 the mean \pm s.e.m. One-way ANOVA with Bonferroni post-test was performed to
801 determine significant differences due to the presence of CIDEA (* P < 0.05; *** P < 0.001).
802 **(I-L)** Coexpression of hLIPIN-1 γ -v5 and CIDEA-HA in Hela cells. **(I)** Representative
803 immunofluorescence images showing LD staining (blue) in Hela cells expressing
804 CIDEA-HA (green) in the presence or absence of hLIPIN-1 γ -v5 (red). 24 hours after
805 overexpression of hLIPIN-1 γ -v5 cells were transfected with pcDNA3.1/Cidea-HA and
806 incubated for further 24 hours. **(J)** Phenotypic distribution in randomly selected cells (n
807 > 50) showing the average values for three independent experiments. **(K)** Co-IP assay in
808 lysates of transfected Hela cells. **(L)** PA-beads binding assay for hLIPIN-1 γ -v5. Each co-
809 IP and PA-binding assay was performed at least in triplicate, producing similar results in
810 each experiment.

811 **Figure 7. Proposed molecular mechanism.** **(A)** CIDEA targets the LD through its C-
812 term amphipathic helix and once diffused to the LD surface, it forms cis CIDEA
813 complexes by interacting through the C-term (126-155) region. When two CIDEA-
814 containing LDs make contact, trans interactions between CIDEA molecules in each
815 droplet can be established, which will facilitate the docking of the LDs. Both the N-term
816 and the C-term would contribute by dimerizing with their counterparts of the neighbour
817 LD. This trans interaction will anchor the CIDEA complexes in the LD-LD contact site,
818 promoting a local enrichment of CIDEA. The monolayers of the two LDs will be
819 maintained at short distance by the CIDEA complex. The amphipathic helices, embedded
820 in the hydrophobic region of the membrane, will interact with the cone-shaped PA,
821 creating a local perturbation in the phospholipid barrier that will increase its permeability
822 to TAG. **(B)** The docking of the amphipathic helix to the membrane could facilitate the
823 integration of TAG molecules within the phospholipid hydrophobic tails. Although the
824 helix will be stabilized with its cationic residues pointing outwards, it will interact with

825 PA molecules in its vicinity, which could be pulled out of the monolayer by the helix
826 molecular dynamics. This could create a transitory discontinuity in the polar barrier that
827 will reduce the energy required to transfer the TAG molecules present in the membrane.
828 This alteration, together with the microenvironment created by the CIDEA complex, will
829 reduce the energy barrier necessary to transfer TAG molecules between LDs, allowing
830 the LD growth by lipid transference.

831 **Video 1. Lipid droplet enlargement in differentiating imBAT cells.** Immortalized
832 brown preadipocytes were induced to differentiate by incubation for 48 + 6 hours with
833 the described differentiation cocktails. The cell displays the characteristic LD
834 enlargement pattern triggered by CIDE proteins, defined by the progressive fusion by
835 lipid transference of the pre-existing LDs.

836 **Video 2. Lipid droplet enlargement induced by CIDEA.** LD dynamics in
837 undifferentiated 3T3-L1 cells 6 hours after infection with adenoviral particles carrying
838 the mouse Cidea gene. After CIDEA induction, the initial individual LDs form stable
839 contacts, reflected by small irregularly-shaped clusters of LDs. These interacting LDs
840 undergo an enlargement process by lipid transference, characterized by the progressive
841 enlargement of the acceptor LD and shrinkage of the donor LD until only a few large LDs
842 remain in the cell.

843

844 **References**

- 845 1. Greenberg AS, Coleman RA, Kraemer FB, McManaman JL, Obin MS, Puri V, et al. The role
846 of lipid droplets in metabolic disease in rodents and humans. *J Clin Invest*. 2011;121(6):2102-10.
- 847 2. Walther TC, Farese RV, Jr. Lipid droplets and cellular lipid metabolism. *Annu Rev*
848 *Biochem*. 2012;81:687-714.
- 849 3. Suzuki M, Shinohara Y, Ohsaki Y, Fujimoto T. Lipid droplets: size matters. *J Electron*
850 *Microsc* (Tokyo). 2011;60 Suppl 1:S101-16.
- 851 4. Cinti S. The adipose organ at a glance. *Dis Model Mech*. 2012;5(5):588-94.
- 852 5. Virtanen KA, Lidell ME, Orava J, Heglind M, Westergren R, Niemi T, et al. Functional
853 brown adipose tissue in healthy adults. *N Engl J Med*. 2009;360(15):1518-25.
- 854 6. Cypess AM, Kahn CR. Brown fat as a therapy for obesity and diabetes. *Curr Opin*
855 *Endocrinol Diabetes Obes*. 2010;17(2):143-9.
- 856 7. Harms M, P. S. Brown and beige fat: development, function and therapeutic potential.
857 *Nat Med*. 2013(10):1252-63.
- 858 8. Wu L, Zhou L, Chen C, Gong J, Xu L, Ye J, et al. Cidea controls lipid droplet fusion and lipid
859 storage in brown and white adipose tissue. *Science China Life sciences*. 2014;57(1):107-16.
- 860 9. Puri V, Konda S, Ranjit S, Aouadi M, Chawla A, Chouinard M, et al. Fat-specific protein
861 27, a novel lipid droplet protein that enhances triglyceride storage. *J Biol Chem*.
862 2007;282(47):34213-8.
- 863 10. Puri V, Ranjit S, Konda S, Nicoloso SM, Straubhaar J, Chawla A, et al. Cidea is associated
864 with lipid droplets and insulin sensitivity in humans. *Proc Natl Acad Sci U S A*. 2008;105(22):7833-
865 8.
- 866 11. Xu L, Zhou L, Li P. CIDE proteins and lipid metabolism. *Arterioscler Thromb Vasc Biol*.
867 2012;32(5):1094-8.
- 868 12. Kuerschner L, Moessinger C, Thiele C. Imaging of lipid biosynthesis: how a neutral lipid
869 enters lipid droplets. *Traffic*. 2008;9(3):338-52.
- 870 13. Wilfling F, Wang H, Haas JT, Krahmer N, Gould TJ, Uchida A, et al. Triacylglycerol
871 synthesis enzymes mediate lipid droplet growth by relocating from the ER to lipid droplets. *Dev*
872 *Cell*. 2013;24(4):384-99.
- 873 14. Bostrom P, Andersson L, Rutberg M, Perman J, Lidberg U, Johansson BR, et al. SNARE
874 proteins mediate fusion between cytosolic lipid droplets and are implicated in insulin sensitivity.
875 *Nat Cell Biol*. 2007;9(11):1286-93.
- 876 15. Gong J, Sun Z, Wu L, Xu W, Schieber N, Xu D, et al. Fsp27 promotes lipid droplet growth
877 by lipid exchange and transfer at lipid droplet contact sites. *J Cell Biol*. 2011;195(6):953-63.
- 878 16. Lugovskoy AA, Zhou P, Chou JJ, McCarty JS, Li P, Wagner G. Solution structure of the
879 CIDE-N domain of CIDE-B and a model for CIDE-N/CIDE-N interactions in the DNA fragmentation
880 pathway of apoptosis. *Cell*. 1999;99(7):747-55.
- 881 17. Wang X, Zhang B, Xu D, Gao J, Wang L, Wang Z, et al. Purification, crystallization and
882 preliminary X-ray crystallographic analysis of the CIDE-N domain of Fsp27. *Acta Crystallogr Sect*
883 *F Struct Biol Cryst Commun*. 2012;68(Pt 12):1529-33.
- 884 18. Sun Z, Gong J, Wu H, Xu W, Wu L, Xu D, et al. Perilipin1 promotes unilocular lipid droplet
885 formation through the activation of Fsp27 in adipocytes. *Nat Commun*. 2013;4:1594.
- 886 19. Lee SM, Jang TH, Park HH. Molecular basis for homo-dimerization of the CIDE domain
887 revealed by the crystal structure of the CIDE-N domain of FSP27. *Biochemical and biophysical*
888 *research communications*. 2013;439(4):564-9.
- 889 20. Liu K, Zhou S, Kim JY, Tillison K, Majors D, Rearick D, et al. Functional analysis of FSP27
890 protein regions for lipid droplet localization, caspase-dependent apoptosis, and dimerization
891 with CIDEA. *Am J Physiol Endocrinol Metab*. 2009;297(6):1395-413.
- 892 21. Christianson JL, Boutet E, Puri V, Chawla A, Czech MP. Identification of the lipid droplet
893 targeting domain of the Cidea protein. *Journal of lipid research*. 2010;51(12):3455-62.

- 894 22. Hinson ER, Cresswell P. The antiviral protein, viperin, localizes to lipid droplets via its N-
895 terminal amphipathic alpha-helix. *Proc Natl Acad Sci U S A*. 2009;106(48):20452-7.
- 896 23. Krahmer N, Guo Y, Wilfling F, Hilger M, Lingrell S, Heger K, et al. Phosphatidylcholine
897 synthesis for lipid droplet expansion is mediated by localized activation of CTP:phosphocholine
898 cytidyltransferase. *Cell Metab*. 2011;14(4):504-15.
- 899 24. Barneda D, Frontini A, Cinti S, Christian M. Dynamic changes in lipid droplet-associated
900 proteins in the "browning" of white adipose tissues. *Biochim Biophys Acta*. 2013;1831(5):924-
901 33.
- 902 25. Jambunathan S, Yin J, Khan W, Tamori Y, Puri V. FSP27 promotes lipid droplet clustering
903 and then fusion to regulate triglyceride accumulation. *PLoS One*. 2011;6(12):e28614.
- 904 26. Grahn TH, Zhang Y, Lee MJ, Sommer AG, Mostoslavsky G, Fried SK, et al. FSP27 and PLIN1
905 interaction promotes the formation of large lipid droplets in human adipocytes. *Biochemical and*
906 *biophysical research communications*. 2013;432(2):296-301.
- 907 27. Harms M, Seale P. Brown and beige fat: development, function and therapeutic
908 potential. *Nature medicine*. 2013;19(10):1252-63.
- 909 28. Zhou Z, Yon Toh S, Chen Z, Guo K, Ng CP, Ponniah S, et al. Cidea-deficient mice have lean
910 phenotype and are resistant to obesity. *Nat Genet*. 2003;35(1):49-56.
- 911 29. Fei W, Shui G, Zhang Y, Krahmer N, Ferguson C, Kapterian TS, et al. A role for
912 phosphatidic acid in the formation of "supersized" lipid droplets. *PLoS Genet*.
913 2011;7(7):e1002201.
- 914 30. Wang H, Zhang J, Qiu W, Han GS, Carman GM, Adeli K. Lipin-1gamma isoform is a novel
915 lipid droplet-associated protein highly expressed in the brain. *FEBS Lett*. 2011;585(12):1979-84.
- 916 31. Marrink SJ, Risselada HJ, Yefimov S, Tieleman DP, de Vries AH. The MARTINI force field:
917 coarse grained model for biomolecular simulations. *The journal of physical chemistry B*.
918 2007;111(27):7812-24.
- 919 32. Mohammadyani D, Tyurin VA, O'Brien M, Sadovsky Y, Gabrilovich DI, Klein-Seetharaman
920 J, et al. Molecular speciation and dynamics of oxidized triacylglycerols in lipid droplets: Mass
921 spectrometry and coarse-grained simulations. *Free radical biology & medicine*. 2014;76:53-60.
- 922 33. Rubio-Cabezas O, Puri V, Murano I, Saudek V, Semple RK, Dash S, et al. Partial
923 lipodystrophy and insulin resistant diabetes in a patient with a homozygous nonsense mutation
924 in CIDEC. *EMBO Mol Med*. 2009;1(5):280-7.
- 925 34. Henry SA, Kohlwein SD, Carman GM. Metabolism and regulation of glycerolipids in the
926 yeast *Saccharomyces cerevisiae*. *Genetics*. 2012;190(2):317-49.
- 927 35. Wu C, Zhang Y, Sun Z, Li P. Molecular evolution of Cide family proteins: novel domain
928 formation in early vertebrates and the subsequent divergence. *BMC Evol Biol*. 2008;8:159.
- 929 36. Rose K, Rudge SA, Frohman MA, Morris AJ, Engebrecht J. Phospholipase D signaling is
930 essential for meiosis. *Proc Natl Acad Sci U S A*. 1995;92(26):12151-5.
- 931 37. Choi HS, Su WM, Morgan JM, Han GS, Xu Z, Karanasios E, et al. Phosphorylation of
932 phosphatidate phosphatase regulates its membrane association and physiological functions in
933 *Saccharomyces cerevisiae*: identification of SER(602), THR(723), AND SER(744) as the sites
934 phosphorylated by CDC28 (CDK1)-encoded cyclin-dependent kinase. *J Biol Chem*.
935 2010;286(2):1486-98.
- 936 38. Choi HS, Su WM, Han GS, Plote D, Xu Z, Carman GM. Pho85p-Pho80p phosphorylation
937 of yeast Pah1p phosphatidate phosphatase regulates its activity, location, abundance, and
938 function in lipid metabolism. *J Biol Chem*. 2012;287(14):11290-301.
- 939 39. Han GS, O'Hara L, Carman GM, Siniosoglou S. An unconventional diacylglycerol kinase
940 that regulates phospholipid synthesis and nuclear membrane growth. *J Biol Chem*.
941 2008;283(29):20433-42.
- 942 40. Fakas S, Konstantinou C, Carman GM. DGK1-encoded diacylglycerol kinase activity is
943 required for phospholipid synthesis during growth resumption from stationary phase in
944 *Saccharomyces cerevisiae*. *J Biol Chem*. 2010;286(2):1464-74.

- 945 41. Santos-Rosa H, Leung J, Grimsey N, Peak-Chew S, Siniossoglou S. The yeast lipin Smp2
946 couples phospholipid biosynthesis to nuclear membrane growth. *EMBO J.* 2005;24(11):1931-41.
- 947 42. Adeyo O, Horn PJ, Lee S, Binns DD, Chandrabhas A, Chapman KD, et al. The yeast lipin
948 orthologue Pah1p is important for biogenesis of lipid droplets. *J Cell Biol.* 2011;192(6):1043-55.
- 949 43. Fakas S, Qiu Y, Dixon JL, Han GS, Ruggles KV, Garbarino J, et al. Phosphatidate
950 phosphatase activity plays key role in protection against fatty acid-induced toxicity in yeast. *J*
951 *Biol Chem.* 2011;286(33):29074-85.
- 952 44. Sandager L, Gustavsson MH, Stahl U, Dahlqvist A, Wiberg E, Banas A, et al. Storage lipid
953 synthesis is non-essential in yeast. *J Biol Chem.* 2002;277(8):6478-82.
- 954 45. Han GS, Carman GM. Characterization of the human LPIN1-encoded phosphatidate
955 phosphatase isoforms. *J Biol Chem.* 2010;285(19):14628-38.
- 956 46. Rosell M, Kaforou M, Frontini A, Okolo A, Chan YW, Nikolopoulou E, et al. Brown and
957 white adipose tissues: intrinsic differences in gene expression and response to cold exposure in
958 mice. *Am J Physiol Endocrinol Metab.* 2014;306(8):E945-64.
- 959 47. Hallberg M, Morganstein DL, Kiskinis E, Shah K, Kralli A, Dilworth SM, et al. A functional
960 interaction between RIP140 and PGC-1alpha regulates the expression of the lipid droplet protein
961 CIDEA. *Mol Cell Biol.* 2008;28(22):6785-95.
- 962 48. Risselada HJ, Grubmuller H. How SNARE molecules mediate membrane fusion: recent
963 insights from molecular simulations. *Curr Opin Struct Biol.* 2012;22(2):187-96.
- 964 49. Gubern A, Casas J, Barcelo-Torns M, Barneda D, de la Rosa X, Masgrau R, et al. Group
965 IVA phospholipase A2 is necessary for the biogenesis of lipid droplets. *J Biol Chem.*
966 2008;283(41):27369-82.
- 967 50. Andersson L, Bostrom P, Ericson J, Rutberg M, Magnusson B, Marchesan D, et al. PLD1
968 and ERK2 regulate cytosolic lipid droplet formation. *J Cell Sci.* 2006;119(Pt 11):2246-57.
- 969 51. Kooijman EE, Chupin V, Fuller NL, Kozlov MM, de Kruijff B, Burger KN, et al. Spontaneous
970 curvature of phosphatidic acid and lysophosphatidic acid. *Biochemistry.* 2005;44(6):2097-102.
- 971 52. Arisawa K, Ichi I, Yasukawa Y, Sone Y, Fujiwara Y. Changes in the phospholipid fatty acid
972 composition of the lipid droplet during the differentiation of 3T3-L1 adipocytes. *J Biochem.* 2013.
- 973 53. Hörl G, Wagner A, Cole LK, Malli R, Reicher H, Kotzbeck P, et al. Sequential synthesis and
974 methylation of phosphatidylethanolamine promote lipid droplet biosynthesis and stability in
975 tissue culture and in vivo. *J Biol Chem.* 2011;286(19):17338-50.
- 976 54. Yu J, Zhang S, Cui L, Wang W, Na H, Zhu X, et al. Lipid droplet remodeling and interaction
977 with mitochondria in mouse brown adipose tissue during cold treatment. *Biochimica et*
978 *biophysica acta.* 2015;1853(5):918-28.
- 979 55. Mottillo EP, Balasubramanian P, Lee YH, Weng C, Kershaw EE, Granneman JG. Coupling
980 of lipolysis and de novo lipogenesis in brown, beige, and white adipose tissues during chronic
981 beta3-adrenergic receptor activation. *Journal of lipid research.* 2014;55(11):2276-86.
- 982 56. Bertin R. Glycerokinase activity and lipolysis regulation in brown adipose tissue of cold
983 acclimated rats. *Biochimie.* 1976;58(4):431-4.
- 984 57. Bertin R, Andriamihaja M, Portet R. Glycerokinase activity in brown and white adipose
985 tissues of cold-adapted obese Zucker rats. *Biochimie.* 1984;66(7-8):569-72.
- 986 58. Portet R, Laury MC, Bertin R, Senault C, Hluszko MT, Chevillard L, et al. Hormonal
987 stimulation of substrate utilization in brown adipose tissue of cold acclimated rats. *Proceedings*
988 *of the Society for Experimental Biology and Medicine Society for Experimental Biology and*
989 *Medicine (New York, NY).* 1974;147(3):807-12.
- 990 59. Kiskinis E, Chatzeli L, Curry E, Kaforou M, Frontini A, Cinti S, et al. RIP140 represses the
991 "brown-in-white" adipocyte program including a futile cycle of triacylglycerol breakdown and
992 synthesis. *Molecular endocrinology (Baltimore, Md).* 2014;28(3):344-56.
- 993 60. Whittle A, Relat-Pardo J, Vidal-Puig A. Pharmacological strategies for targeting BAT
994 thermogenesis. *Trends Pharmacol Sci.* 2013;34(6):347-55.
- 995 61. Krahmer N, Farese RV, Jr., Walther TC. Balancing the fat: lipid droplets and human
996 disease. *EMBO Mol Med.* 2013;5(7):973-83.

997 62. Li H, Song Y, Li F, Zhang L, Gu Y, Jiang L, et al. Identification of lipid droplet-associated
998 proteins in the formation of macrophage-derived foam cells using microarrays. *Int J Mol Med*.
999 2010;26(2):231-9.

1000 63. Zhou L, Xu L, Ye J, Li D, Wang W, Li X, et al. Cidea promotes hepatic steatosis by sensing
1001 dietary fatty acids. *Hepatology*. 2012;56(1):95-107.

1002 64. Matsusue K, Kusakabe T, Noguchi T, Takiguchi S, Suzuki T, Yamano S, et al. Hepatic
1003 steatosis in leptin-deficient mice is promoted by the PPARgamma target gene Fsp27. *Cell Metab*.
1004 2008;7(4):302-11.

1005 65. Arnold K, Bordoli L, Kopp J, Schwede T. The SWISS-MODEL workspace: a web-based
1006 environment for protein structure homology modelling. *Bioinformatics*. 2006;22(2):195-201.

1007 66. Maupetit J, Derreumaux P, Tuffery P. PEP-FOLD: an online resource for de novo peptide
1008 structure prediction. *Nucleic Acids Res*. 2009;37(Web Server issue):W498-503.

1009 67. Trott O, Olson AJ. AutoDock Vina: improving the speed and accuracy of docking with a
1010 new scoring function, efficient optimization, and multithreading. *J Comput Chem*.
1011 2009;31(2):455-61.

1012 68. Monticelli L, Kandasamy SK, Periole X, Larson RG, Tieleman DP, Marrink SJ. The MARTINI
1013 Coarse-Grained Force Field: Extension to Proteins. *J Chem Theory and Comput*. 2008;4(5):819-
1014 34.

1015 69. Berendsen HJC, Postma JPM, van Gunsteren WF, DiNola A, R. HJ. Molecular dynamics
1016 with coupling to an external bath.
1017 *Journal of Chemical Physics*. 1984;81(8):3684-90.

1018 70. Humphrey W, Dalke A, Schulten K. VMD: visual molecular dynamics. *J Mol Graph*.
1019 1996;14(1):33-8, 27-8.

1020 71. Van Der Spoel D, Lindahl E, Hess B, Groenhof G, Mark AE, Berendsen HJ. GROMACS: fast,
1021 flexible, and free. *Journal of computational chemistry*. 2005;26(16):1701-18.

1022 72. Manifava M, Thuring JW, Lim ZY, Packman L, Holmes AB, Ktistakis NT. Differential
1023 binding of traffic-related proteins to phosphatidic acid- or phosphatidylinositol (4,5)-
1024 bisphosphate-coupled affinity reagents. *J Biol Chem*. 2001;276(12):8987-94.

1025 73. Brachmann CB, Davies A, Cost GJ, Caputo E, Li J, Hieter P, et al. Designer deletion strains
1026 derived from *Saccharomyces cerevisiae* S288C: a useful set of strains and plasmids for PCR-
1027 mediated gene disruption and other applications. *Yeast*. 1998;14(2):115-32.

1028 74. Carpenter AE, Jones TR, Lamprecht MR, Clarke C, Kang IH, Friman O, et al. CellProfiler:
1029 image analysis software for identifying and quantifying cell phenotypes. *Genome Biol*.
1030 2006;7(10):R100.

1031 75. Gaspar ML, Aregullin MA, Jesch SA, Henry SA. Inositol induces a profound alteration in
1032 the pattern and rate of synthesis and turnover of membrane lipids in *Saccharomyces cerevisiae*.
1033 *J Biol Chem*. 2006;281(32):22773-85.

1034

Figure 1

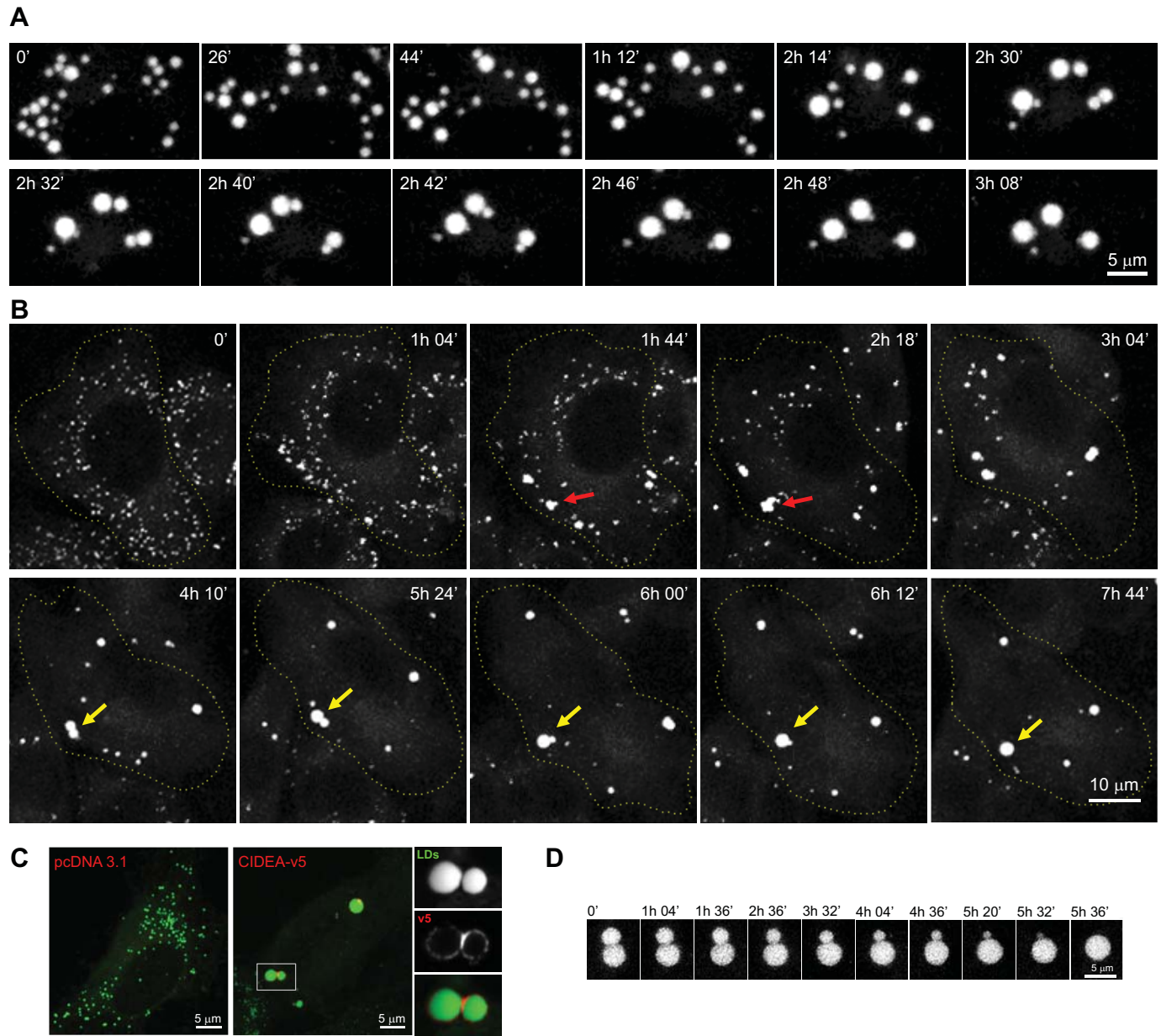
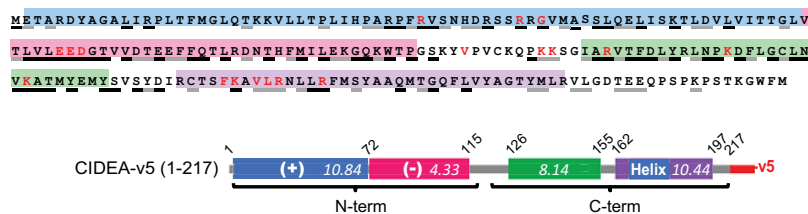
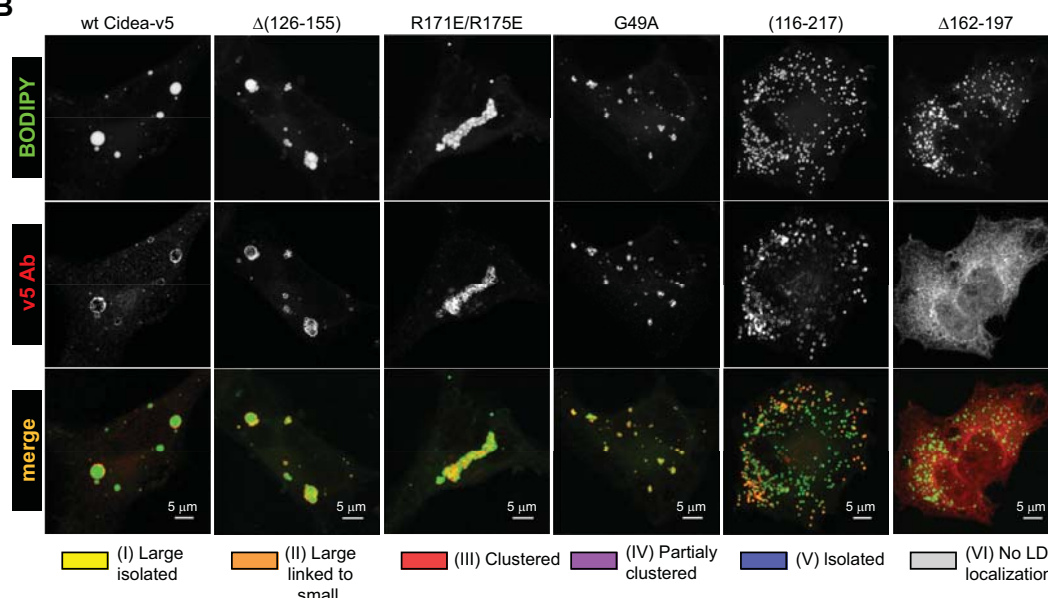


Figure 2

A



B



C

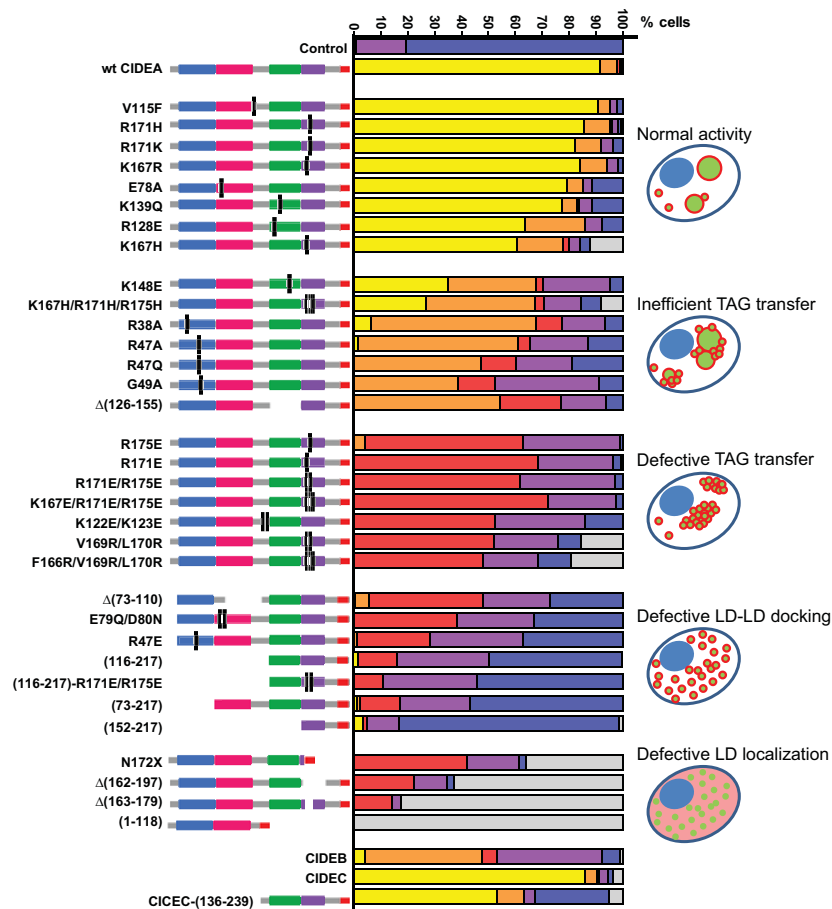


Figure 3

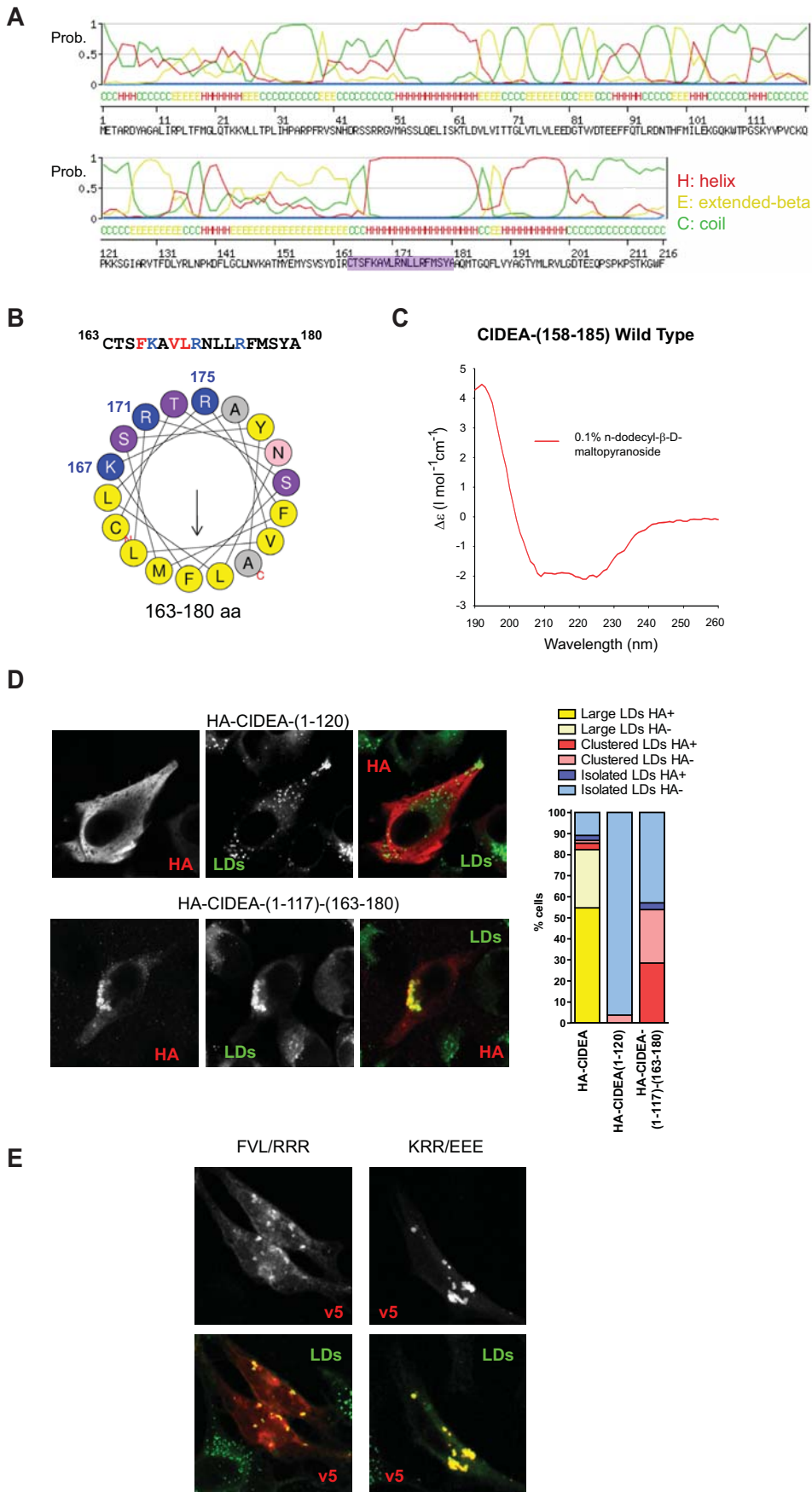


Figure 4

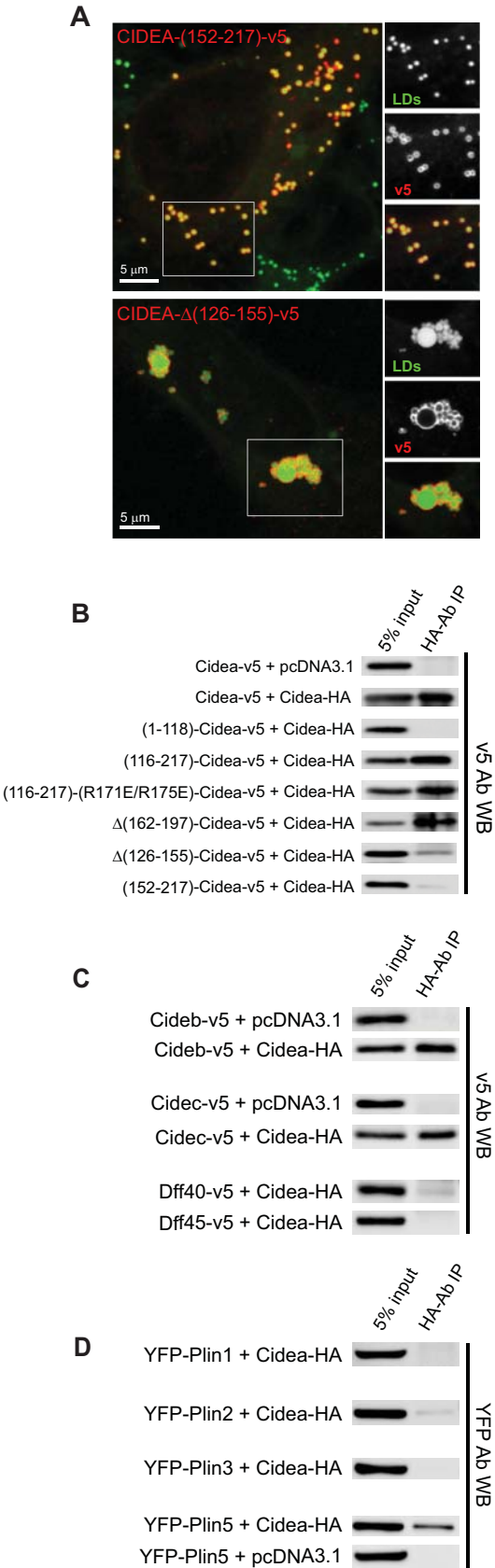


Figure 5

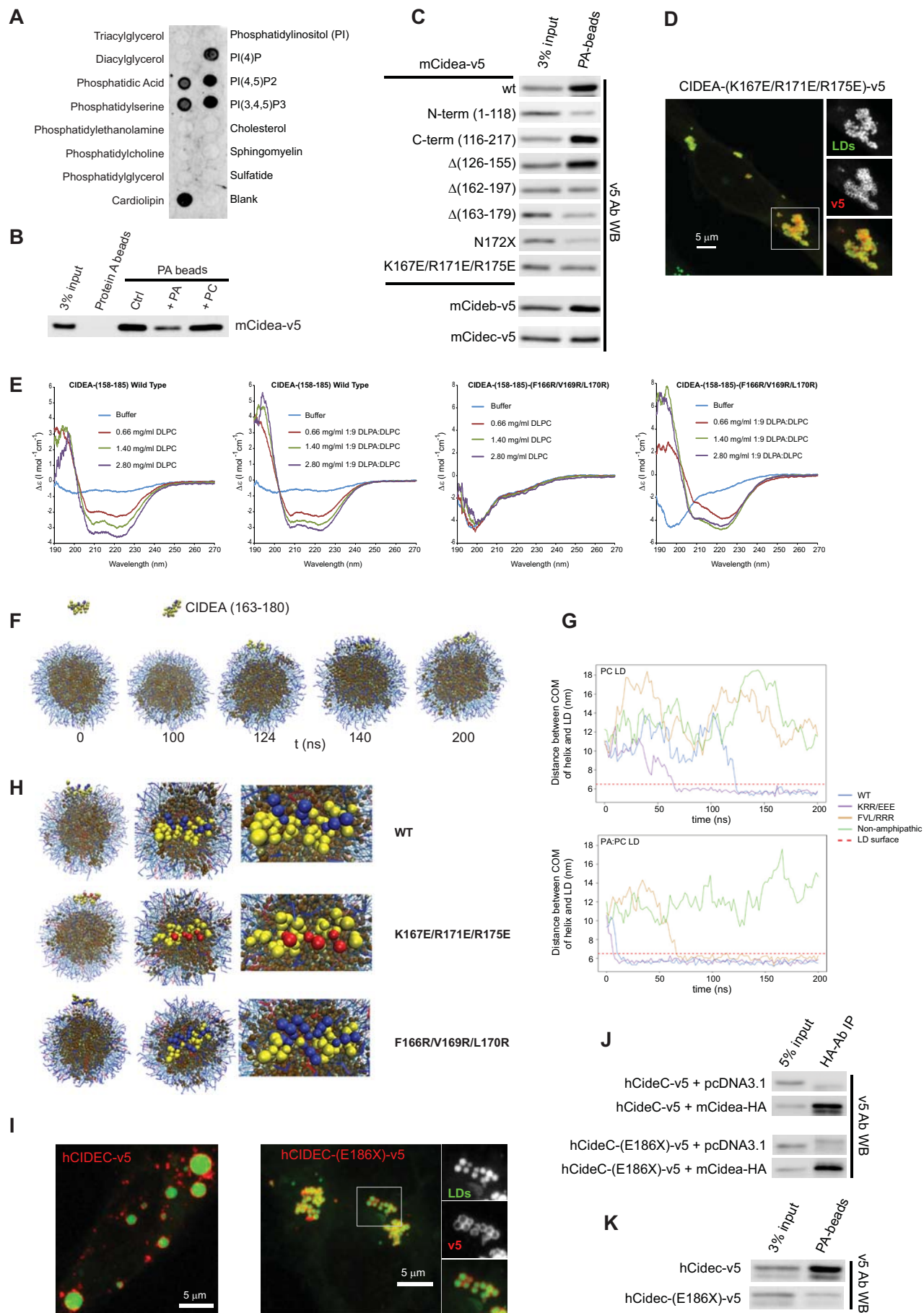


Figure 6

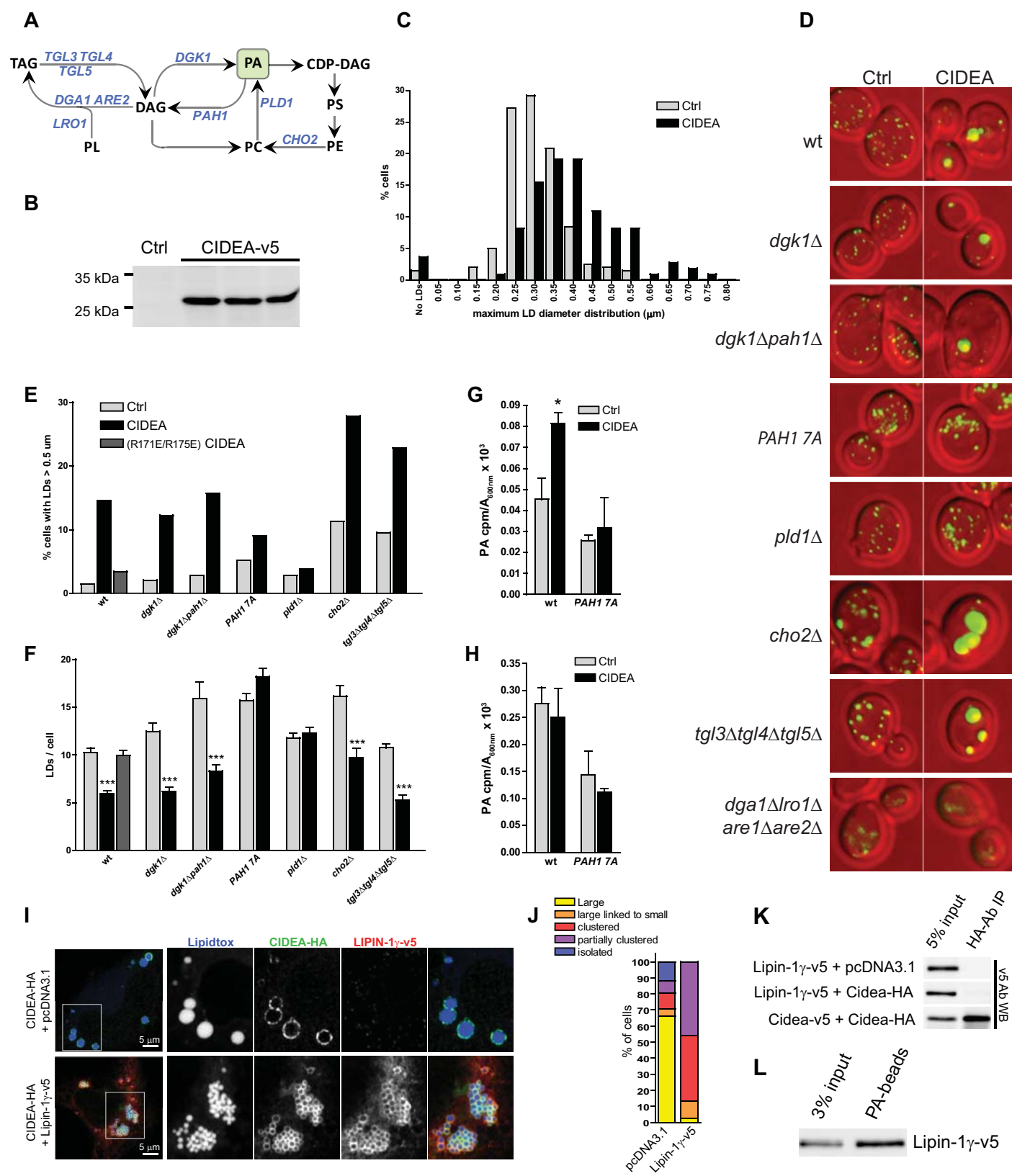
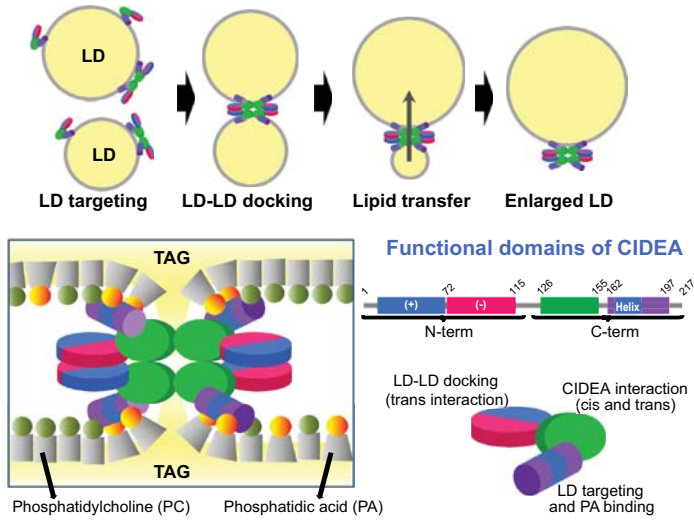


Figure 7

A



B

